Atmospheric Particle Budget
in a Remote Marine Environment

by

Jennifer Ruth Eden

A thesis submitted in partial fulfillment
of the requirements for the degree of

Master of Science

University of Washington

1995

Approved by Melvin Baker
Chairperson of Supervisory Committee

Program Authorized
to Offer Degree Geophysics Program

Date June 6, 1995

In presenting this thesis in partial fulfillment of the requirements for a Master's degree at the University of Washington, I agree that the Library shall make its copies freely available for inspection. I further agree that extensive copying of this thesis is allowable only for scholarly purposes, consistent with "fair use" as prescribed in the U.S. Copyright Law. Any other reproduction for any purposes or by any means shall not be allowed without my written permission.

Signature Jennifer R Eden

Date June 6, 1995

Table of Contents

List of Figures

List of Tables

Acknowledgements

I am grateful to many people for their support and guidance during graduate school. First and foremost, I appreciate Professor Marcia Baker's advice and support. She has always presented me with interesting and provactive questions which guided my research through the years. I am grateful to my committee members, Professor Dean Hegg and Professor Conway Leovy for their insight and suggestions throughout this project. I am grateful to Dr. Anthony Clarke for allowing me to use his ASTEX particle data, and for providing helpful suggestions regarding this data set. Many thanks to Robert Pincus for facilitating my work through his knowledge of relevant software, hardware, and the ASTEX data set; to Phil Austin for help with *airubc* software; to Robert Solomon for answering all of my computer-related questions; to Derek Coffman for use of his nucleation code; and to Dr. Eric Jensen for use of his coagulation code.

I am grateful to numerous funding sources for their financial support of my graduate education: NASA Space Grant, the University of Washington Geophysics Program, and the NASA Aerosol Interdisciplinary Program Grant NAGW-3754.

Abundant thanks go to my very supportive family and friends. They all knew my abilities better than I and fed me encouragement religiously. Special thanks to Roxane Ronca for being a very special friend; to Cecilia Bitz, Margaret Rozendaal, Kirsten Lorentzen and Nadine Cutler for sharing laughter and anxiety on many noontime runs. My mother and parents-in-law have provided endless parental support. And, my husband, Stuart Willick put up with me, pulled me through, and loved me anyhow.

Dedication

For my husband Stuart

Who has supported me and loved me despite it all

Chapter 1: Introduction

Recent focus on the possibility of global warming has led the field of atmospheric science and climate studies in many directions. It has become painfully evident that for every process which we understand there are a handful of other, related processes about which we are ignorant. The study of particulate matter in the atmosphere is one such example. An understanding of climate requires that we understand the atmospheric properties which affect the earth's radiative balance: namely, substances which scatter, absorb and transmit radiation. The substances in the atmosphere which affect radiative transfer are gases (H_2O_{vap}, O_3, CO_2, etc.), liquid and solid particles, and clouds (which are composed of water condensed on particles). The radiative properties of clouds, in turn, are dependent on the droplet size spectrum which is dependent on the number of suitable particles (cloud condensation nuclei, CCN) on which water can condense. Clearly, an understanding of climate requires a detailed understanding of atmospheric particulates (Hobbs, 1993).

Although aerosols (any liquid or solid substance suspended in a gas) have been studied for decades in laboratory settings and the processes which affect aerosol properties in the laboratory are relatively well-understood (Fuchs, 1964), the application of this understanding to atmospheric aerosols is far from complete. The goal of this study is to quantify which processes control the size, concentration, and composition of the particulate component of the atmospheric aerosol in a remote marine environment. Our focus on the remote marine environment is based on the desire to understand the unpolluted, background environment. A firm understanding of the unpolluted environment will provide a basis onto which one can add anthropogenic perturbations.

Currently, most observations of atmospheric particles in the marine environment have been made in the marine boundary layer (MBL). The generally observed characteristics of particles in the MBL are discussed in review articles by Heintzenberg (1989) and Fitzgerald (1991). The submicron particle number concentration is relatively constant (~100-300/cc) and is predominantly composed of non-sea salt sulfate (nss-sulfate). This implies a steady state situation in which source processes must balance sink processes.

Hoppel, *et. al.* (1990) propose that an *in situ* source of submicron particles, namely homogeneous nucleation, is necessary to balance the loss of small particles due to coagulation and depositional growth at a rate of 10-100 particles cm^{-3} day^{-1}.

The submicron size distribution is bimodal: one peak is at ~0.03 μm radius and is primarily due to gas to particle conversion (GPC); the other peak is at ~ 0.1 μm and is thought to be due to in cloud oxidation of SO_2. Particles with radii greater than 0.5 μm (coarse particle mode) are primarily composed of sea salt whose production is strongly dependent on wind speed. Although coarse particles only constitute 5-10% of total particle number, they comprise 90-95% of the total particle mass.

Particle properties in the marine free troposphere (the region of the troposphere above the marine boundary layer) have not been investigated much. In fact, Fitzgerald's 1991 review article on marine aerosols has no discussion of particles in the free troposphere (FT). The only extensive observational study of submicron particles in the marine FT is presented by Clarke (1993) from data taken during the Global Backscatter Experiment 2 (GLOBE2). The results from this experiment display regions of elevated particle concentrations (predominantly sulfuric acid) high in the FT. Clarke assumes these elevated concentrations are due to nucleation of gases in the upper FT (8-10 km). Clarke proposes that subsidence must eventually bring these recently nucleated particles into the MBL thus contributing to the particle properties in the MBL. Covert, *et. al.* (1995) also observe indirect evidence of particle production in the FT through use of air parcel back trajectories. They find that elevated ultrafine particle concentrations in the Pacific MBL are associated with air which has recently subsided from the FT (within 5 days).

Numerous modelling studies demonstrate the theoretical relationships among various particle source and sink processes in the MBL (Hegg, *et. al.*, 1992a; Hegg, *et. al.*, 1992b; Lin, *et. al.*, 1992; Raes and VanDingenen, 1992; Raes, 1995). Very few of these modelling efforts have been verified observationally and only Raes (1995) includes processes in the FT.

I would like to complete an observation-based analysis of submicron particle data in both the FT and the MBL in order to quantify which particle processes are the most

important determinants of particle concentration, size, and composition. Through the quantification of dominant processes, I can validate or dispute current ideas (both observational and model based) about nucleation in the MBL (Hoppel, *et. al.*, 1990) or the FT (Clarke, 1993); about evolution of particle size distributions due to coagulation or gaseous diffusion; and about transport processes.

Achievement of this goal requires an extensive data set with particle data, thermodynamic data, winds, and gas concentrations. The most suitable data set for completion of this project is from the Atlantic Stratocumulus Transition Experiment (ASTEX) conducted in June, 1992. The ASTEX Lagrangian missions afford us the opportunity to follow an air mass over several days and thus observe particle evolution. The observed particle evolution can then be used to complete a remote marine atmosphere particle budget study using particle concentration as the evolving variable of interest.

A particle budget study is based on the premise that particle sources and sinks must account for observed particle concentrations, n, according to the conservation equation, $\frac{dn}{dt} = S_{ource}(n) - S_{ink}(n)$. If I can quantify all relevant source and sink processes (discussed in Chapter 2), then I can compute how the particle concentration changes in a given region due to the sources and sinks acting upon it (Figure 1.1). A bud-

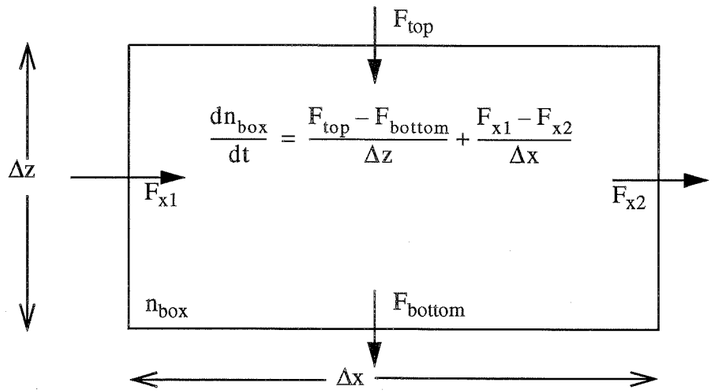

F_i: particle fluxes

Figure 1.1 Schematic of budget calculation for one box.

get study assumes that particle concentrations within each box are homogeneous. If the budget does not reproduce the observed concentrations, one can evaluate the importance of unmeasurable processes by determining the magnitude of the sources or sinks necessary to balance the particle budget. In either case, the budget study will help illuminate which processes are the dominant contributors to the observed particle properties. The results thus obtained can be used to parameterize dominant processes for use in computer models and can demonstrate which processes need to be examined more thoroughly in future experiments.

In the following chapters I will discuss particle process theory, the ASTEX data set and analysis methods. I will follow this background information with discussion of an Eulerian case study (June 10, 1992) and a Lagrangian case study (June 12-14, 1992). I chose these two case studies because they are the most complete data sets from unpolluted flights during ASTEX. I will present an analysis of observed elevated concentration zones, ECZs (similar to those seen by Clarke, 1993), and discuss the possibility of nucleation and particle evolution related to these ECZs. Finally, I will present the particle budget analysis using data from the Lagrangian case study and discuss implications of the budget results for future research.

Chapter 2: Particle Processes

Sub-micron particle concentrations and masses are determined by the processes which the particles experience. The relationship linking the sources and sinks to the property ξ (mass or concentration) of particles in size class i is called a conservation equation for ξ and has the form:

$$\frac{d\xi_i}{dt} = S_{ource}\left(\xi_i\right) - S_{ink}\left(\xi_i\right) \qquad (2\text{-}1)$$

$$\xi = \{n \text{ (conc.)}, m \text{ (mass)}\}$$

There are a number of known source and sink processes for atmospheric particles upon which I will elaborate in this chapter.

2.1 PARTICLE SOURCE AND SINK PROCESSES

I will discuss all known source and sink processes starting with those which are most relevant to the smallest particles and moving to those which are important for larger particles. Some of the processes discussed below cannot be evaluated with the ASTEX data set, but they may represent missing terms in the budget study and are therefore important to understand.

2.1.1 Nucleation

Nucleation is used here to describe the formation of sub-micron particles from gases in the atmosphere. Although atmospheric gas molecules are continually colliding, stable aggregates of molecules will only occur when growth processes are more probable than decay processes. The factors which determine nucleation rates are temperature, relative humidity, gas species and concentrations, and pre-existing surface area.

Nucleation products are smaller (radius ~ 1 nm) than can be observed with current instrumentation. Consequently, the nucleation process cannot be directly observed: rather, we have to rely on theoretical predictions and measurements of those factors which control nucleation to infer the rate of nucleation. Within the constraints of classical theory, nucleation rates can be predicted given measurements of sub-micron particle size distributions; measurements of relative humidity, sulfuric acid concentrations and ammonia con-

centrations (Coffman and Hegg, 1995); and measurements of pre-existing particle surface area.

2.1.2 Coagulation

Coagulation describes particle growth due to inelastic collisions with other particles. Particles in one size range are shifted to a larger size range during collisions according to a coagulation kernel, K (cm^3/s), which is dependent on the sizes of the particles in question. Thus, the particle size distribution is controlled by Equation 2-2 (Pruppacher and Klett, 1978).

$$\frac{dn_k}{dt} = \frac{1}{2}\sum_{i=1}^{k-1} K_{i,k-i} n_i n_{k-i} - n_k \sum_{i=1}^{\infty} K_{ik} n_i \qquad (2\text{-}2)$$

The two terms in Equation 2-2 are: production of k-sized particles (n_k) due to coagulation of particles smaller than size k, and depletion of n_k due to coagulation of k-sized particles with other particles. As can be seen in Equation 2-2, one must know both particle concentrations and sizes to assess coagulation rates. Particles whose radii range from 0.01 - 0.1 μm are most likely formed by coagulation of smaller particles because this is a size range in which neither direct production from nucleation nor surface-derived sources is efficient (Twomey, 1977).

2.1.3 Vapor diffusion

Diffusion is the redistribution of any substance (ξ) due to molecular collisions. The diffusion equation describes this phenomenon,

$$\frac{\partial \xi}{\partial t} = D\nabla^2 \xi \qquad (2\text{-}3)$$

where D is the diffusion coefficient in m^2/s. In the context of particle processes, diffusion refers to diffusion of gases onto existing particles.

The rate of change of particle size due to diffusion of gases (*g*) to or from the particle surface is determined by the diffusion coefficient, D, and the gradient in gas concentration between the surface of the particles and the surrounding environment. The rate of

change in the concentration of particles of size r_i due to diffusional growth is denoted by Equation 2-4.

$$\frac{dn}{dt} = -\frac{\partial}{\partial r}(\dot{r}n)\Big|_{r_i} \qquad (2\text{-}4)$$

$$\text{where } \dot{r}_i = \frac{D_g \rho_{sat,g} S_g}{\rho_L r_i} \qquad (2\text{-}5)$$

In Equation 2-5, $\rho_{sat,g}(kg/m^3)$ is the density of gas *g*, when saturated with respect to the particle; S_g is the supersaturation of gas *g* over the particle, $S_g \equiv (\rho_g/\rho_{sat,g}) - 1$; and $\rho_L(kg/m^3)$ is the density of the particle. In order to assess the effect of diffusion on particle concentration, one needs information on the sizes, concentrations, and composition of particles as well as detailed, spatially-resolved measurements of the relevant gas concentrations.

2.1.4 Turbulent dispersion of particles

Turbulent dispersion of particles is a result of turbulent mixing with surrounding air on a variety of spatial scales. This process in often parameterized by the diffusion equation (Pasquill, 1974). The dispersion rate can be assessed if one can determine a value of *K*, the effective diffusion coefficient. For homogeneous, isotropic turbulence, we can use a length scale, *l**, of eddies that are most effective in mixing to express *K* as:

$$K \sim v^*(l^*) \cdot l^*. \qquad (2\text{-}6)$$

In order to find a value for *K* we must find a value for *v*(l*)*, the velocity which is characteristic of eddies acting on length scale *l**. We can find an expression for *l** and *v*(l*)* through observation of the turbulent velocity spectrum of the observed environment which can be used in the diffusion equation to assess the rate of change of particle concentration due to turbulent dispersion.

2.1.5 Deposition

Dry deposition simply describes particle removal from a given region due to grav-

itational sedimentation. This process depends only on the deposition velocity of the particles, v_{dep}, and the size of the region that they must pass through in order to be removed. The deposition velocity of submicron particles is a function of particle size and local winds and is tabulated by Huebert, *et. al.*, 1995. According to tabulated deposition velocities, dry deposition is negligible for particles smaller than 0.4 μm diameter. Any determination of the magnitude of deposition processes is dependent on particle size but independent of particle concentration.

2.1.6 Cloud Processing

Cloud processing describes all particle sources and sinks due to the presence of clouds. The processes which this term subsumes are: incorporation of particles into cloud droplets (a sink); precipitation (a sink); evaporation of cloud droplets (a source of large particles due to many small particles coagulating within the cloud droplets); and growth due to in-cloud oxidation (a source or sink depending on the size range). In order to assess the magnitude of these sources and sinks one needs information about the concentrations of particles in and out of cloudy regions as well as detailed information about cloud properties (droplet concentration and size, cloud lifetime, cloud extent, etc.). Even with this information, it is difficult to come up with definitive conclusions about the effect of cloud processes on particle populations, largely because each of these processes is governed by multiple elementary processes. For example, incorporation of particles into cloud droplets includes coagulation of particles with droplets; collection of particles due to droplet motion; and, preliminarily, development of particles into cloud condensation nuclei.

2.1.7 Transport

Transport refers to particles moving from one region to another due to winds. We can describe transport as a sum: transport by mean winds plus transport by the turbulent wind component as expressed in Equation 2-7 for the component of the wind (u) in the *i* direction.

$$\overline{u_i n} = \overline{(\bar{u}_i + u_i') \cdot (\bar{n} + n')} = \bar{u}_i \bar{n} + \overline{u_i' n} \qquad (2\text{-}7)$$

In Equation 2-7, the first term on the far right hand side is the flux due to mean transport and the second term is the flux due to turbulent transport, i.e., turbulent mixing. The gradient of the particle flux describes how the particle concentration changes in time due to transport (Equation 2-8).

$$\frac{dn}{dt} = \frac{d\left(\bar{u}_i \bar{n}\right)}{dx_i} + \frac{d\left(\overline{u_i' n'}\right)}{dx_i} \qquad (2\text{-}8)$$

When speaking about transport processes, the frame of reference in which the observations were taken is significant, as expressed in the two terms on the right hand side of Equation 2-9: the first is the Eulerian term which describes the change in particle concentration in time as observed from a fixed frame of reference; the second is the Lagrangian component which describes how the particle concentration varies spatially due to advection when viewed from within the reference frame of the moving parcel.

$$\frac{dn_i}{dt} = \frac{\partial n_i}{\partial t} + \vec{u} \cdot \vec{\nabla} n_i \qquad (2\text{-}9)$$

The only measurements which are needed to assess horizontal and vertical transport of particles are horizontal and vertical winds, and particle concentrations.

2.1.8 Sea salt production

Sea salt particle production is determined by wind shear across the ocean surface. If winds are strong enough to create whitecaps, then sea salt particles can be produced due to bursting whitecap bubbles or due to spume drops, i.e., drops produced by the wind's disruption of wave crests (Monahan, *et. al.*, 1986). Consequently, researchers often find a correlation between wind speed and particle concentration near the sea surface (O'Dowd and Smith, 1993; Smith, *et. al.*, 1993).

In order to assess the magnitude of the sea salt source observationally, one must determine what portion of the observed particle population is salt. Sea salt and other surface derived substances (dust, soot) are refractory, i.e., they do not burn off when heated to high temperatures. Refractory particle concentrations are measured during ASTEX (Sec-

tion 4.1.2). Thus, if I can assume that the measured refractory particle concentrations are indeed sea salt, then I can treat the refractory particle concentration as sea salt and compute sea salt fluxes accordingly.

2.2 Characteristic Time Scales

Each particle process can be discussed in terms of a characteristic time, τ, as expressed in Equation 2-10. The characteristic times can then be used as a basis for determining the relative importance of the various processes which may be controlling the particle size distribution.

$$\tau_{process} = \bar{n}_i \times \left(\left. \frac{dn_i}{dt} \right|_{process} \right)^{-1} \qquad (2\text{-}10)$$

2.3 Summary

The previous discussion details the equations I must solve and the variables needed in order to assess each of the above processes observationally. Unfortunately, some of these variables are not easily obtained with current technology and funds. Consequently, there is no single data set which contains all of the terms necessary to complete this analysis and, hence, the analysis discussed in the following pages is limited to those processes which can be evaluated using available data. The importance of some of the processes which I am unable to evaluate may be inferred through use of the particle budget.

Chapter 3: ASTEX Data Set

ASTEX (Atlantic Stratocumulus Transition Experiment) was an international experiment which was conducted near the Azore Islands in the Atlantic Ocean in June of 1992 (Bluth and Albrecht, 1993a,b). A triangular region north of the Azores was observed for most of the month of June by ship, aircraft, land-based sites, and satellite. Aircraft are the most useful platforms from which to assess the particle budget because they can be used to measure particle concentrations and sizes at many elevations. In the following pages I will discuss why I chose to use data from the ASTEX field project and the advantages and disadvantages of this data set. The focus of my research is defined by the constraints of this data set.

3.1 Advantages

The sheer amount and variety of instrumentation used during ASTEX makes the ASTEX data set exceptional among currently available remote marine atmosphere data sets. This feature, along with the attempted cross-coverage between observation platforms, makes ASTEX the most useful experiment to date if one is attempting to describe any aspect of the lower marine atmosphere in a complete sense. I want to describe the evolution of submicron particle size distributions which requires knowledge of particle properties, gas properties, the synoptic environment, and dynamic and thermodynamic conditions.

During ASTEX, three aircraft, four ships and multiple satellites covered the field site extensively. This coverage produced an unusually high density of observations. Most missions were designed to take advantage of the multiple observation platforms by having aircraft fly over ships and multiple aircraft flying side-by-side or vertically separated. Each platform had a large variety of instrumentation to measure synoptic conditions, thermodynamic conditions, dynamical conditions and particle and gas information. (See Chapter 4 for instrumentation details.) When two or more platforms were carrying the same instrumentation there was an effort to intercompare the results in order to assess the reliability and accuracy of the instrumentation. The ships were able to carry more instru-

mentation than the aircraft and were able to provide boundary conditions for the entire experiment.

Finally, there was an attempt during ASTEX to conduct two Lagrangian experiments in order to observe the evolution of an air mass in time. The goal in these missions was to follow an airmass through the field area for two to three days over a trajectory that did not cross any of the islands. When such a circumstance was predicted, a ship at the upwind end of the field site released passive balloons as air tracers. The aircraft then proceeded to take turns following these balloons throughout a two to three day period. The ships attempted to sail beneath the air trajectory at multiple times throughout the Lagrangian missions.

Intensive satellite coverage and ECMWF-derived winds of the ASTEX region provide us with satellite images (visible and infrared), wind fields, and pressure fields for the ASTEX region and the surrounding North Atlantic during June, 1992.

3.2 Disadvantages

3.2.1 Particle measurements

As one expects with observational programs, there were difficulties during ASTEX. The single largest shortcoming in terms of studying particle evolution was that not all platforms measured particles in the same size ranges. The three aircraft used were the NCAR Electra, the British C130 and the University of Washington C131-A. The Electra flew CN counters operated by Dr. A. Clarke which measure number concentrations in the size range 3 nm to 3 μm. Clarke also used laser optical particle counters (OPC) to measure particle size distributions from 0.14 to 7.0 μm and a differential mobility analyzer (DMA) to measure size distributions from 0.02-0.55 μm. The C130 used an ASASP instrument to measure particle concentrations in size bins ranging from 0.1 μm to 3.0 μm. The lower end of this size range is two orders of magnitude too large to be able to observe nucleation products. The C131-A used multiple instruments to cover the entire particle size range from 3 nm to 10 μm. They also used a differential mobility particle system (DMPS) to assess size distributions from a filter pack every few minutes. Unfortunately, the C131-A had no measurements of vertical winds which renders it impossible to assess

vertical transport for the C-131 data. Given the relative attributes of the instrumentation on the various aircraft, I chose to focus on data obtained on the Electra aircraft.

3.2.2 Gas measurements

During ASTEX, the only high frequency gas measurements taken on aircraft were ozone and water vapor concentrations. Other gases which are particularly important in determining particle growth due to gaseous diffusion are: sulfur dioxide (SO_2), hydroxyl radical (OH), sulfuric acid (H_2SO_4), ammonium (NH_3), and methanesulfonic acid (MSA). Most of these gases exist in very low concentrations in the atmosphere and are consequently difficult to measure. The best gas data available during ASTEX were taken on participating ships which use filter packs to obtain samples over a few hours (Huebert, *et. al.*, 1995; Blomquist, *et. al.*, 1995). The only one of the aforementioned gas concentrations measured on aircraft was SO_2. OH and H_2SO_4 were not measured due to the lack of available technology when ASTEX occurred.

3.2.3 Flight plan

The ASTEX mission was planned with the intent of observing the transition from stratocumulus clouds to trade cumulus clouds. This has little to do with my goal, which is to understand which processes control submicron particle properties. Consequently, the ASTEX flight plans are not ideally suited to the examination of particle properties.

Even if ASTEX had been designed to examine particle processes, the flight plans would likely have been insufficient given the fact that the importance of transport processes over short length scales (<100 km) had not been realized prior to this study. The difficulty with the ASTEX flight plans is that they do not permit evaluation of horizontal turbulent flux gradients. I can analyze vertical turbulent flux gradients using stacked flight legs, but horizontally parallel flight legs were generally not flown. I am also unable to assess horizontal divergence because closed flight paths in the horizontal plane were not flown.

3.3 Research Focus

The factors noted in the above discussion limit the scope of my research. I cannot assess diffusion of gases onto existing particles and cloud processing. I can make only

crude order of magnitude estimates for time scales for nucleation and turbulent dispersion of particles. The terms I can address most definitively are: coagulation; deposition; mean transport (vertical and horizontal); turbulent vertical mixing; and sea salt production. Consequently, these terms are the major focus of my research and, fortunately, they appear to be dominant particle processes in the unpolluted ASTEX environment.

Chapter 4: Analysis Methods

In this chapter, I will discuss the instruments and methods which I use to complete the analysis discussed in the following chapters.

4.1 DATA FILTERING

4.1.1 Microphysical and thermodynamic data

The Electra aircraft carried instruments capable of taking a wide array of microphysical and thermodynamic data at various frequencies (see Table 4.1). I average all Electra data to 1 Hz for use in the following analyses.

The most uncertain variable which we use frequently is vertical velocity. As listed in Table 4.1, the uncertainty is ± 0.05 m/s. Typical measured values of vertical velocity range between - 0.2 m/s and + 0.2 m/s. Clearly, the uncertainty is very significant. There is also some occurrence of offset in the vertical velocity measurements which may be on the order of - 0.1 m/s for the ASTEX flights which I am analyzing. The magnitude of the offset can be determined by calculating mean vertical velocities on high altitude ferry flight legs. Any difference between the mean value and zero can be considered the systematic offset. An offset will affect mean values of vertical velocity ($\overline{w}$) but not the variation about the mean ($w'=w-\overline{w}$).

For the ASTEX flights which I examine, the mean vertical velocity along ferry legs is non-zero and negative (~ - 0.18 m/s) for the initial ferry leg, and close to zero (~ - 0.04 m/s) for the final ferry leg of each flight. Consequently, it is not clear what the offset should be for these flights or whether, in fact, there is an offset. I will assume there is no offset and will analyze the data without modification due to this. This decision appears physically reasonable when one examines soundings of volatile particles in the following chapters and notices the dramatic increase in particle concentration with elevation.

These uncertainties affect calculations of vertical transport. Mean vertical particle fluxes ($\overline{w}\,\overline{n}$) are highly uncertain because of both the uncertainty and the offset. I will assume that the offset is zero and thus the only inaccuracies in mean vertical fluxes are due to the uncertainties. The uncertainty in mean particle fluxes is

Table 4.1: Electra instrumentation
(Miller and Friesen, 1988) Note: still waiting for info. on uncertainties!

Name	Units	Frequency	Description
Latitude & Longitude	degree	1 Hz	Inertial Navigation System resolution: 0.0014°
Static Pressure (p)	mb	20 Hz	Rosemount Model 1501 static pressure corrected for local flow distortion
Ambient Temperature (T_a)	C	20 Hz	Calculated from total temperature and dynamic heating using conservation of energy for a perfect gas undergoing adiabatic processes.
Dew/frost point (T_d)	C	1 Hz	EG&G Model 137 dew point hygrometer
Aircraft True Airspeed	m/s	20 Hz	Calculated using conservation of energy similar to case for ambient temperature
Winds (horiz. & vert)	speed: m/s direction: deg	20 Hz	Calculated from INS parameters and aircraft airspeed and attack/sideslip angles accuracy: ± 0.05 m/s
Potential Temperature (θ)	K	20 Hz	Calculated: $\theta = T_a\left(\frac{1000}{p}\right)^{R/c_p}$
Equivalent Pot. Temp. (θ_e)	K	20 Hz	Calculated: $\theta_e = \theta \times f(Q_{tot}, T_{lcl})$ T_{lcl} = lifting condensation level
Relative Humidity (RH)	%	1 Hz	Calculated: $RH = \frac{e}{e_s} \times 100$ e = atmospheric water vapor pressure
Water Mixing Ratio (Q_{tot})	g-H_2O/kg-air	1 Hz	Calculated: $Q_{tot} = 622\frac{e}{p-e}$
Geometric Radar Altitude	m	1 Hz	APM-159 resolution: 1.86 m

$$\sigma_{\overline{w}\overline{n}} = \pm\overline{w}\overline{n}\sqrt{\left(\frac{0.05}{\overline{w}}\right)^2 + \left(\frac{10}{\overline{n}}\right)^2} \approx \pm\overline{w}\overline{n}\left|\frac{0.05}{\overline{w}}\right|. \qquad (4\text{-}1)$$

This uncertainty is of significant magnitude but will not tend to alter the sign of the resultant flux. Consequently, this uncertainty will not change the observed trends and source and sink regions. Nevertheless, keep in mind that all values of mean vertical transport may be uncertain. In the case studies (Chapter 5 and 6) I will discuss individual instances which appear erroneous and illustrate the physical effect of applying an offset to vertical velocities.

Turbulent vertical particle fluxes ($\overline{w'n'}$) are only affected due to the uncertainty in the vertical velocity value. We consider the sign of w' to be robust, even if the absolute value is not. This assumption is based on the fact that we have averaged the wind speeds from 20 Hz to 1 Hz thus eliminating high frequency anomalies. Thus, we can assume that turbulent vertical fluxes are quite robust.

4.1.2 Particle data

Clarke operated a number of instruments on board the Electra aircraft which measure particle concentrations and size distributions (see Table 4.2). The concentration data were recorded at approximately 0.1 Hz. Consequently, in order to use these data with the rest of the Electra data set, I interpolate the Clarke data to 1 Hz resolution using the cubic spline method. The size distribution data were taken every few minutes and are not resolved to 1 Hz.

The instruments which Clarke uses for measuring particle concentrations are condensation nuclei counters. Two CN counters (diameter range: 15 nm - 3.0 μm) were operated: one at 25°C (called CN); the other at 300°C (called RCN). Thermal pretreatment of a particle sample can indicate particle composition, as it reflects the vaporization behaviour of various species. The RCN counter measures those particles which are refractory at 300°C, that is surface derived particles such as dust, sea salt, and soot (Clarke, 1991). In the marine environment, sea salt is the primary component of the surface derived particles. The difference between the CN concentration and the RCN concentration is the component of the CN concentration which did burn off at 300°C, that is, the volatile component (VCN). In the marine environment, the primary component of the volatile particle concentration is sulfate. Clarke also operated an ultrafine CN counter (UCN, diameter range:

Table 4.2: Clarke instrumentation
(Clarke, *et. al.*, 1995)

Name	Units	Diameter Range	Uncertainty	Description
Condensation Nuclei Counter (CN)	#/cc	0.015-3.0 μm	± 10/cc	Thermal Systems Inc., 3760 Counts total particle number in designated size range by laser detection; particles are enlarged due to water uptake for easier observation
Refractory CN counter (RCN)	#/cc	0.015-3.0 μm	± 10/cc	Thermal Systems Inc., 3760 CN counter perated at 300 ° C to burn off volatile particles
Ultrafine CN counter (UCN)	#/cc	0.003-3.0 μm	± 20/cc	Thermal Systems Inc., 3025 Same operation as CN counter over larger size range
Laser optical particle counter (OPC)	#/cc/ size bin	256 channel resolution for 0.14-7.0 μm size range		Particle Measurement System LAS-X Optical counter operated at low RH to observe dry mass; aerosol preheated to infer composition. (Clarke, 1991; Porter, *et. al.*, 1992)
Scanning differential mobility analyzer (DMA)	#/cc/ size bin	17 size bins in 0.02-0.55 μm size range		Thermal Systems Inc., 3071 Similar analysis to OPC over different size range

3 nm - 3.0 μm) at 25°C. The difference between the UCN concentration and the CN concentration is the component of the particle concentration which is ultrafine in size, that is a diameter range of 3 nm - 15 nm. The UCN counter is not operated at high temperatures because of particle loss so I do not have a measure of whether the ultrafine particles are volatile or refractory. From here on, any reference to UCN refers only to those particles with diameters between 3 nm and 15 nm as determined from subtracting the CN concentration from the UCN concentration. See Table 4.3 for definitions of particle acronyms.

The CN and UCN counters give erroneous values in cloud due to water shattering on the probe. Therefore, Clarke recommends that all CN data at relative humidities above 90% be removed. He also finds that the ultrafine CN counter overmeasured concentrations by a factor of 1.9. I modified the data according to these recommendations.

Table 4.3: Definition of Particle Acronyms

Name	Size range (diameter)	Definition
CN	15 nm - 3 μm	Measured: all particles at 25°C
RCN	15 nm - 3 μm	Measured: all particles at 300°C
VCN	15 nm - 3 μm	VCN = CN - RCN Those particles which burn off at 300°C
UCN	3 nm - 15 nm	$UCN = UCN_{measured} - CN$

4.2 Dispersion of Particles

In order to analyze particle dispersion, I complete the analysis outlined in Section 2.1.4. This entails calculating spectra for vertical wind speed and for eastward and northward components of horizontal wind speed. The spectrum routine removes high lag points from the covariance of wind speed and then applies a Tukey window to the covariance in order to reduce the effects of the edges of the data on the high frequency component of the spectrum. The Fourier transform of the covariance is the power spectrum in frequency space which is modified to the power spectrum in wavenumber space. The power spectrum in wavenumber space is then used to analyze dispersion according to Section 2.1.4.

4.3 Coagulation

I explore the occurrence of coagulation for observed particle concentrations using a coagulation code written by Eric Jensen at NASA Ames Research Center. In order to use this code for regimes where particle sizes are smaller than or comparable to the mean free path of the gas molecules (i.e., Knudsen number greater than 1), I modified Jensen's calculation of the coagulation kernel according to Sitarski & Seinfeld (1977).

The Jensen code uses log-normal size distributions as input. These are calculated from a peak radius, total concentration, and standard deviation of the distribution. The log-normal distribution is split into a fixed number of size bins. Each successive bin doubles the volume of the previous bin, starting at a designated minimum radius. Coagulation kernels are calculated for every possible two particle interaction. The size distribution is then produced for each time step, assuming all particles have the same composition,

according to the coagulation equation (Equation 2-2). The inclusion of the free molecular and transitional regimes (Kn > 1, Sitarski & Seinfeld (1977)), requires input of the particle mass density. Pressure and temperature are also input parameters.

I use observed concentrations as input. Since I often only know how many UCN and CN particles are present, I find the peak radius and total concentration under the log-normal curve(s) by trial and error. I assume that the input log-normal distribution must have the same concentration in the 3 nm - 15 nm range as is measured by the UCN counter, and the same concentration in the 15 nm - 3 μm range as is measured by the VCN counter. Occassionally size distributions are available which I use to determine whether a monomodal or bimodal distribution is most realistic. I can examine forward and backward evolution of a given observation by finding which distribution fits observations and then stepping forward in time, or, by trial and error, seeing from which particle distribution the observed distribution could have been produced.

4.4 TRANSPORT

Transport calculations contain three parts: calculation of mean and turbulent fluxes; calculation of relevant flux gradients; and calculation of transport times from the flux gradients.

4.4.1 Fluxes

Flux is defined as the amount of tracer, ξ, (particle concentration, mass, heat, etc.) crossing a unit area per unit time as expressed in Equation 2-7. To calculate the mean and turbulent particle fluxes discussed in Section 2.1.7 I use the following procedure:

1. Truncation of each flight leg to a 60 km segment.
2. Removal of mean from each variable (i.e., wind, particle concentration).
3. Calculate mean flux: Mean flux = $\overline{u_i}\,\overline{n}$
4. Removal of trend from "de-meaned" data by subtracting best fit line from data.
5. Taper time series to zero over first and last 10% of the data in order to reduce edge effects.
6. Calculate turbulent flux: Turbulent flux = $\overline{u_i'n'}$
7. Separate turbulent flux into those motions occurring on scales less than or

greater than 10 km by filtering the time series in frequency space.

$$\overline{u_i'n'}_{low} = \frac{1}{N}\mathcal{F}^{-1}\{u_i(f_{low})\,n^*(f_{low})\}$$

$$\overline{u_i'n'}_{high} = \frac{1}{N}\mathcal{F}^{-1}\{u_i(f_{high})\,n^*(f_{high})\} \qquad (4\text{-}2)$$

$$f_{low} < \frac{U_{aircraft}}{10\text{ km}};\ f_{high} > \frac{U_{aircraft}}{10\text{ km}}$$

In Equation 4-2, $\mathcal{F}^{-1}$ is the inverse fourier transform, n* is the complex conjugate of n in frequency space, N is the number of data points used for normalization, and $U_{aircraft}$ is the mean velocity of the aircraft.

I obtain four flux values from this analysis: mean flux (step 3); turbulent flux (step 6); turbulent flux for length scales greater than 10 km (low frequency component of step 7); and turbulent flux for length scales less than 10 km (high frequency component of step 7). The total turbulent flux is just the sum of the low and high frequency components of the flux.

This procedure can be used for any wind component perpendicular to the flight direction. Only mean fluxes can be calculated for the wind component parallel to the flight segment.

4.4.2 Gradients

Flux gradients are calculated over spatial regions consistent with the direction of the flux under consideration.

$$\frac{\Delta\left(\overline{u_i}\,\overline{n}\right)}{\Delta x_i} = \frac{\left(\overline{u_i}\,\overline{n}\right)_1 - \left(\overline{u_i}\,\overline{n}\right)_2}{x_{i,1} - x_{i,2}} \qquad (4\text{-}3)$$

$$i = \{\hat{x},\hat{y},\hat{z}\}$$

As denoted in Equation 4-3, gradients must be calculated for flight segments which are parallel to one another in the x_i direction. Thus, gradient calculations are dependent on the set-up of the flight plan as evident in Figure 4.1.

During ASTEX, there are a significant number of vertically separated flight legs, but not of horizontally separated flight legs. Consequently, I can only calculate turbulent horizontal flux gradients for the few flight segments which are horizontally separated and

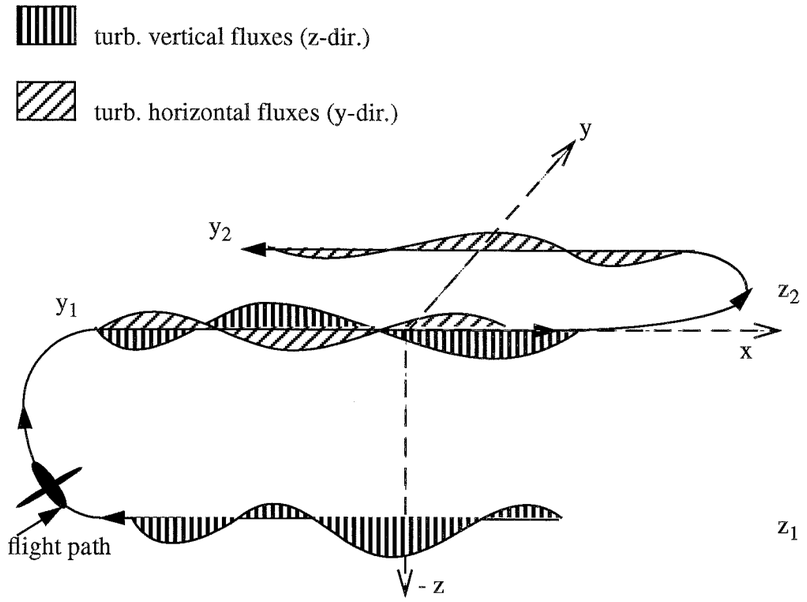

Figure 4.1 Example of flux gradient calculation. The horizontal fluxes are calculated using the component of the horizontal wind which is perpendicular to the flight path. These fluxes can then be compared to fluxes for a flight path parallel but horizontally separated from the original flight path. Vertical flux gradients are calculated in the same fashion but using vertically separated flight legs.

flown within a short time period. I compute mean horizontal fluxes parallel to the flight leg by calculating mean fluxes in the first tenth and last tenth of a 60 km flight segment (without tapering or detrending) and then calculating the gradient. This may be inaccurate due to the fact that the mean values are calculated over just one tenth of a flight leg (i.e., 6 km), which may not be indicative of mean characteristics in this environment.

4.4.3 Cross inversion transport

Above and below the inversion, particle concentrations change due to entrainment as well as due to particle fluxes. Above the inversion, entrainment does not change the particle concentration, it only raises the height of cloud top. Thus, in the region above cloud the particle concentration (n_{CT}) changes only due to the flux into this region (F_{CT})

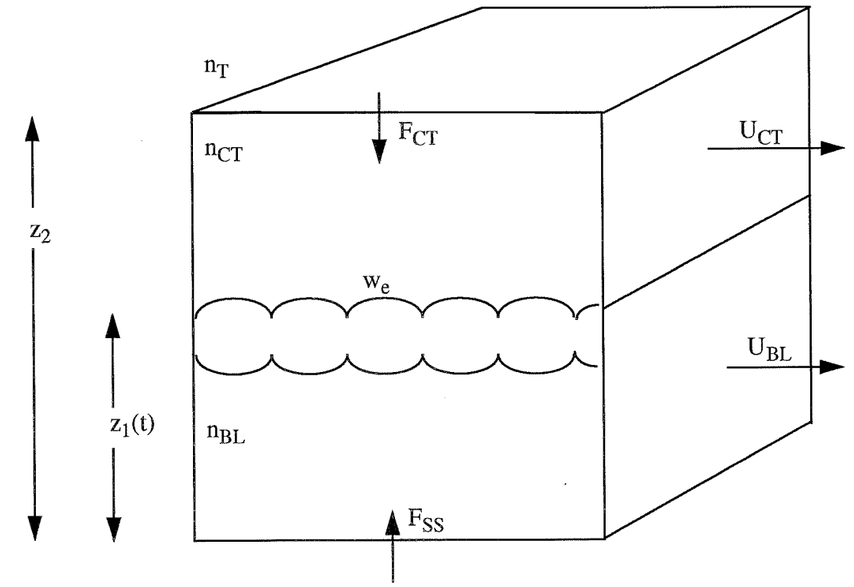

Figure 4.2 Schematic of transport across inversion. Cloud top height, $z_1(t)$, varies with time due to the difference between the entrainment rate and the subsidence rate.

as expressed in Equation 4-4 (see Figure 4.2).

$$\frac{dn_{CT}}{dt} = \frac{F_{CT}}{z_2 - z_1(t)} = \frac{w\,(n_T - n_{CT})}{z_2 - z_1(t)} \qquad (4\text{-}4)$$

Below cloud the particle concentration (n_{BL}) varies in time due to the entrainment rate and other fluxes into the MBL (F_{SS}) according to Equation 4-5 (see Figure 4.2).

$$\frac{dn_{BL}}{dt} = \frac{w_e\,(n_{CT} - n_{BL}) + F_{SS}}{z_1(t)}. \qquad (4\text{-}5)$$

These expressions can be used to calculate transport in the regions adjacent to cloud.

4.4.4 Transport times

Characteristic times are described by Equation 2-10. For the particular case of par-

ticle transport, the characteristic time is defined by

$$\tau_i = \frac{\bar{n}}{\frac{d}{dx_i}(\bar{u}_i\bar{n})} \quad \text{or} \quad \tau'_i = \frac{\bar{n}}{\frac{d}{dx_i}\left(\overline{u_i'n'}\right)} \tag{4-6}$$

for mean and turbulent transport times, respectively. These transport times describe the time it takes for the mean particle concentration in the region over which the gradient was calculated to change by a factor of e due to transport (see Figure 4.3). These characteristic

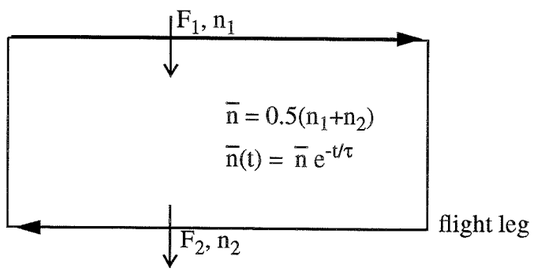

Flux: $F_i = (\overline{w'n'})_i$ or $(\bar{w}\,\bar{n}_i)$

Figure 4.3 Schematic of the significance of transport calculations. Transport times are calculated from the gradient of the fluxes (Equation 4-6). The quantity which changes in a given characteristic time is $\bar{n}$.

transport times will be the dominant component of the budget study in Chapter 8.

4.5 Sea salt production

To assess the strength of the source of sea salt particles it is necessary to identify a portion of the observed particle concentration as sea salt. Without a detailed composition analysis, I must rely upon the refractory nature of salt particles and the fact that the salt particle population should be correlated with wind speed (O'Dowd and Smith, 1993; Smith, *et. al.*, 1993) in order to evaluate whether the particles are composed of salt.

The relationship between RCN concentration and wind speed can be evaluated by computing the correlation between the turbulent vertical RCN flux and the mean horizontal RCN flux in accordance with parameterizations of surface fluxes. If these fluxes are correlated then one can infer that there are surface fluxes of refractory particles. Since the lowest flight segments are flown at 50 m, I do not know definitively whether the surface fluxes are sea salt or some source in between the surface and 50 m, but because there are no obvious alternative refractory particle sources in this region, I will assume the observed refractory particles are sea salt. The mean and turbulent fluxes which I use for the correlation are calculated over 10 km and 1 km flight segments because sea salt production is sporadic so a correlation may not exist over large spatial scales. Once I have verified that the RCN concentration is sea salt, then surface fluxes of RCN are calculated in the same fashion as any other fluxes.

4.6 Trajectories

Three dimensional air trajectories are calculated using a program written by C. Bretherton for use with the ASTEX dataset. This program computes three dimensional trajectories forward or backward in time using ECMWF wind components. The only necessary input data are starting position, pressure, and time.

4.7 Conclusion

In the following chapters I will analyze ASTEX data from June 10, 1992 and from the first Lagrangian mission (June 12-14, 1992) in the fashion outlined above. These results will then be combined in refractory and volatile particle budgets for the Lagrangian mission.

Chapter 5: Case Study, June 10, 1992

In this chapter I will describe the environment on June 10 through use of soundings of particles and of thermodynamic tracers, back trajectories to assess air mass origin, and satellite images for synoptic-scale views of the North Atlantic. I will analyze particle sources and sinks in the marine boundary layer (MBL) and the free troposphere (FT), in the manner discussed in Chapter 4.

On June 10, 1992 the inversion height decreases from 855 mb to 885 mb above broken statocumulus decks over a four hour period in the morning; the region sampled is not influenced by polluted air; and the boundary layer is not well-mixed. Keep in mind that the June 10, 1992 flight is not a Lagrangian mission, so the aircraft does not sample the same air mass throughout the flight. Because the cloud deck is broken, I can discuss the distinction between particle characteristics in cloudy and clear regions.

5.1 SOUNDINGS

Soundings from June 10 (Figure 5.1) show that the inversion early on June 10 (6:20 AM) is high and sharp. A sharp inversion is indicative of strong subsidence. Subsidence is also evident from back trajectories early on June 10 (Section 5.2). Also, on June 10 the MBL below cloud appears to be divided into two subregions and a transitional layer between these layers at about 960 mb. In contrast to the 6:20 sounding, by 10:25 AM the inversion has weakened considerably and lowered and cloud has broken up. The sub-inversion layering still exists although there is no cloud layer. The dew point temperature profile in the free troposphere has a fair amount of structure and variability throughout June 10. The temperature lapse rate in the FT is quite constant.

Winds on June 10 are out of the NW in the upper FT (700-800 mb) and out of the north in the lower FT and MBL (>800 mb). The mean wind speed in the MBL is 4.5 m/s and in the FT is 3.4 m/s. The measured mean vertical wind speed is -0.1 m/s in the MBL, -0.13 m/s in the FT early on June 10, and decreases to - 0.06 m/s later on June 10.

The detailed thermodynamic structure of the BL on June 10 is most easily seen from soundings of equivalent potential temperature (θ_e) and total water mixing ratio (Q) (Figure 5.2). From Figure 5.2 we can justify subdivision of the BL into four layers (three

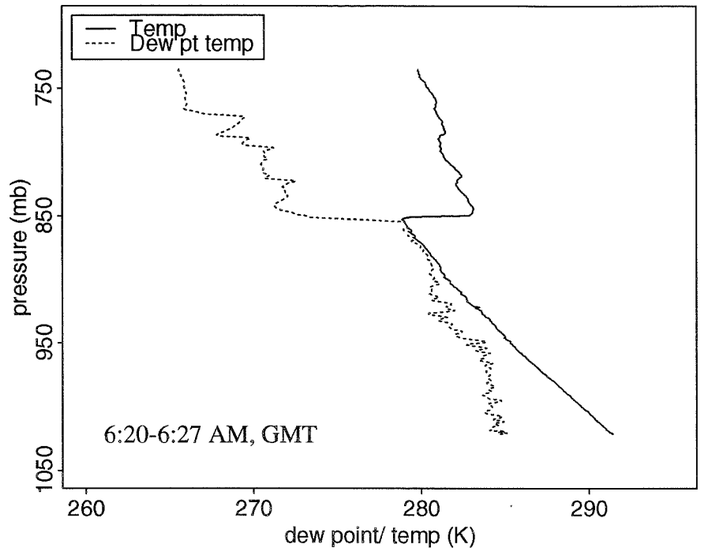

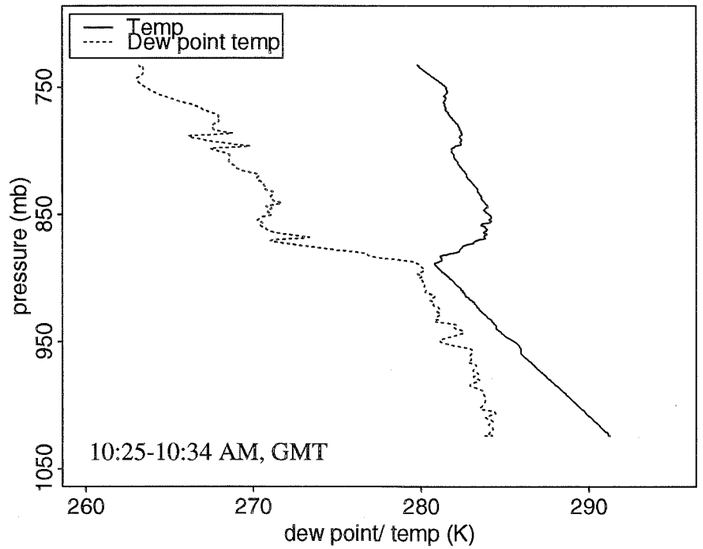

Figure 5.1 June 10, 1992: soundings. 6:20-6:27 AM, GMT and 10:25-10:34 AM, GMT.

layers when no cloud is present): the sea surface layer (SS) from surface to approximately 950 mb; a transition layer (TL) from 950 to 930 mb; the subcloud layer (SL) from 930 to 875 mb; and the cloud layer (CL) from 875 to 853 mb. Each of these layers is relatively well-mixed as is apparent in soundings of total water (Q) and potential temperature (θ_e) (Figure 5.2), except for the TL which appears to be characterized by a gradient between the properties of the SS and SL layers. The SL and CL layers are quite well-mixed in terms of moisture but not in terms of θ_e. Further subdivision of the SL layer may be warranted but I have chosen to use moisture as the parameter which delineates layering. Although these layers (except for the TL) are relatively well-mixed within individual soundings, their characteristics vary over time.

The MBL atmosphere on June 10, 1992 can be described as decoupled. This means that the sea surface, as a source of heat and moisture, is not directly linked to the top of the boundary layer and, hence, the heat and moisture variables in the boundary layer are not well-mixed. Decoupling can occur due to shortwave heating within the cloud layer or evaporation of drizzle beneath the cloud, both of which impede mixing in the boundary layer (Martin, *et. al.*, 1995).

Particle soundings from June 10 indicate the vertical particle distribution as seen in Figure 5.3. Particle properties on June 10 can be described as well-mixed in the boundary layer and variable in the free troposphere. The concentrations of volatile and refractory particles are quite constant with height in the boundary layer at about 200/cc, with refractory concentrations a bit higher than volatile concentrations. In the FT, the trends are not clear. The mean refractory particle concentration is elevated from that in the BL (~300/cc) but the concentration varies quite a bit between 200/cc and 500/cc. The volatile particle concentration in the FT is elevated during one sounding to 600/cc, but is constant and lower (~100/cc) than the concentration in the MBL during the other two soundings. The ultrafine particle concentration during the June 10 soundings is near zero most of the time and thus I did not even present the plot. Because there are few, if any, ultrafine particles, we have no evidence for recent nucleation as a source, except in one small scale elevated concentration zone (ECZ) at 5:37 AM (discussed in Chapter 7).

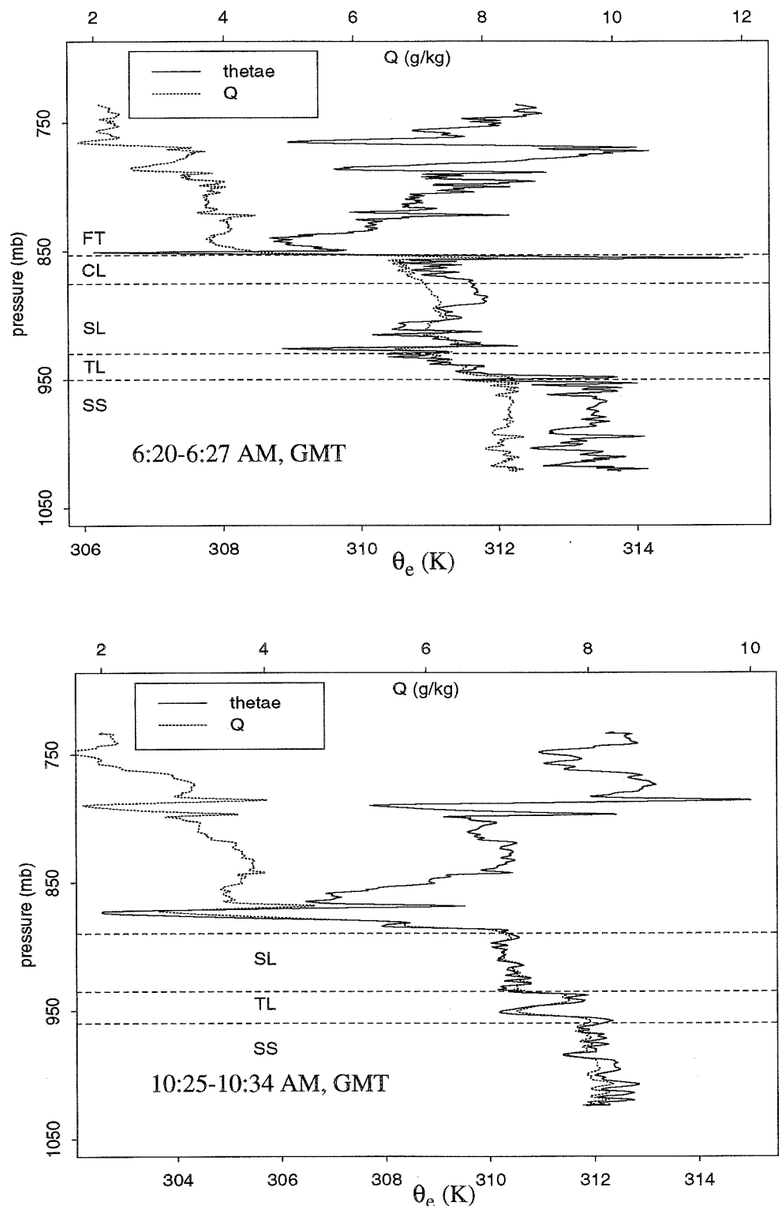

Figure 5.2 Layered structure of atmosphere on 6/10/92.

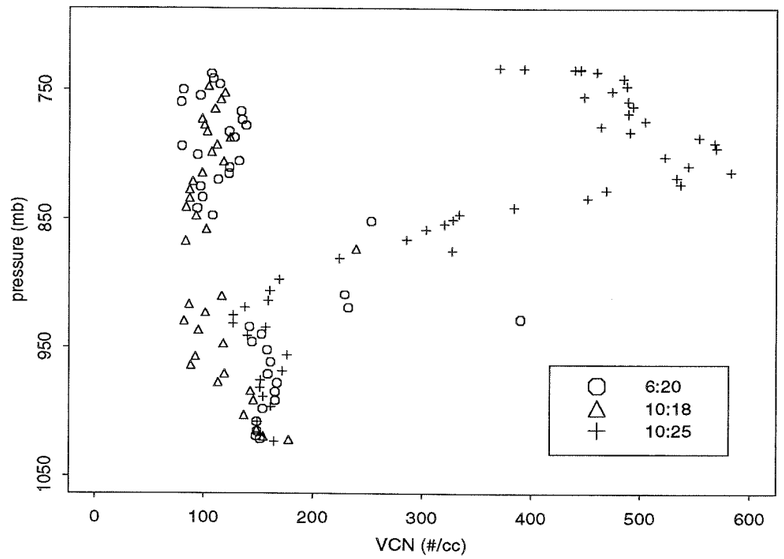

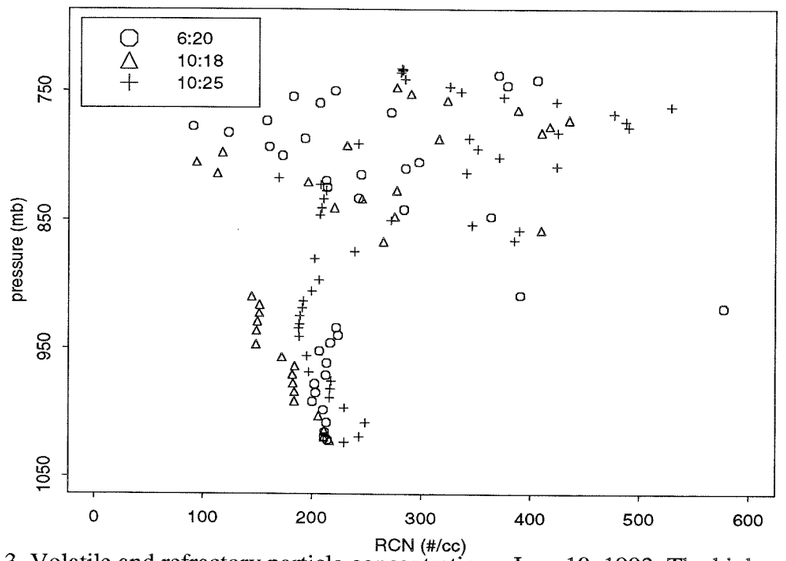

Figure 5.3 Volatile and refractory particle concentrations, June 10, 1992. The high concentrations between 850 mb and 950 mb are likely due to instrument error in/near cloud.

Also evident in these composite particle soundings is some idea of how particle concentrations vary in time. Because the June 10 flight is not Lagrangian, the time variation is not indicative of particle evolution but of different particle characteristics in different environments. The most obvious trend is that both volatile and refractory particle concentrations increase in the FT during the 10:25 sounding. Interestingly, the 10:25 sounding in which the VCN concentration is elevated in the FT occurs over clear skies. This could be due to higher subsidence in clear regions which serves to transport nucleation products from the upper FT down toward the MBL more quickly than in regions of lower subsidence. There is evidence from the back trajectory analysis that subsidence is quite rapid after 8:00 AM, whereas before 8:00 AM the subsidence rate is close to zero. The difficulty with the theory of downward transport of nucleation products in this case is that refractory concentrations are elevated as well as volatile particles. Refractory particles cannot be formed by nucleation. So, in this case, elevated particle concentrations must be due to another source which I cannot assess. The only other apparent time trend is that refractory concentrations in the TL and SL layers decrease from 6:20 to 10:18 AM. The possible reasons for this trend are discussed in Section 5.5.2.

Figure 5.3 shows the particle soundings from 6:20 and 10:25 delineated thermodynamically as in Figure 5.2. This displays the fact that although there is a significant amount of thermodynamic layering in the MBL, there is virtually no layering apparent in particle soundings. This is indicative of the fact that particle concentrations are not linked to thermodynamic tracers.

5.2 BACK TRAJECTORIES

Back trajectory calculations are a helpful means by which to determine the origin of an airmass. Four day back trajectory calculations for June 10 trace MBL and FT air back to remote North America near Newfoundland (-60 W, 50 N) as shown in Figure 5.5. The trajectories are slightly different for air originating in the MBL than for air originating in the FT. MBL air does not move as rapidly as FT air, and it originates a bit farther north than FT air. This implies that the FT air mass was moving quite rapidly from remote North America in order to reach the Azores in four days. The likelihood of pollution orig-

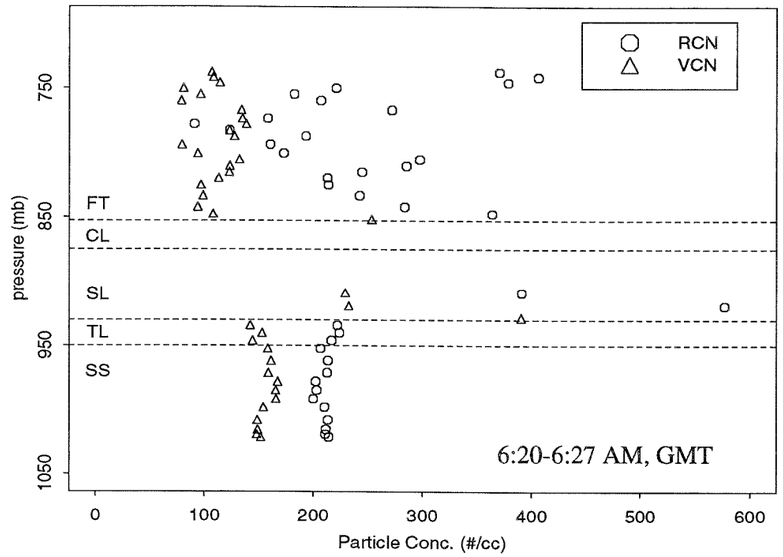

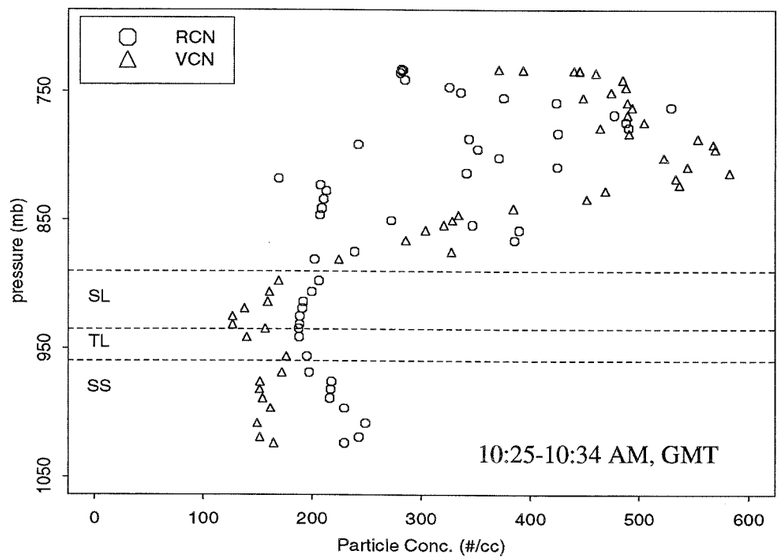

Figure 5.4 Particle concentrations, June 10, 1992 with thermodynamic layers represented. Notice that no layering is apparent.

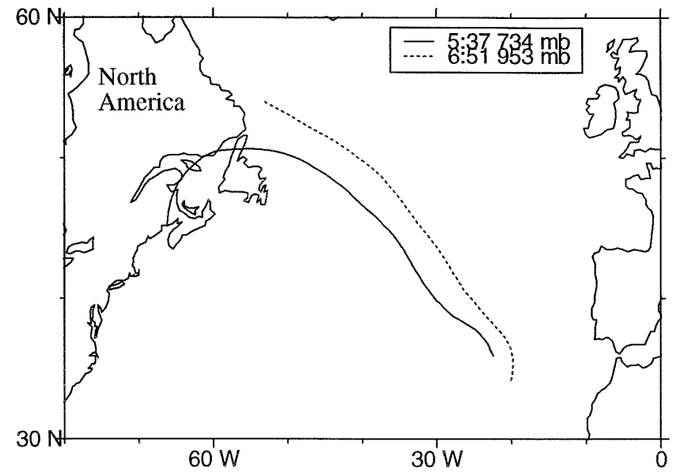

Figure 5.5 Back trajectories from two starting points on June 10, 1992. Notice different origins for air originating within the MBL (6:51) and air originating in the FT (5:37). The 6:51 trajectory is representative of all MBL trajectories, and the 5:37 trajectory is representative of FT trajectories.

inating in the region around Newfoundland is small and pollution is not evident in black carbon data (a pollution tracer).

Subsidence prior to June 10 is quite variable as inferred from the three dimensional back trajectories (not shown). The air parcels which arrive in the ASTEX region prior to 6:00 AM subside by 70 mb over 40 hours, or 0.5 cm/s. The air parcels which arrive in the ASTEX region after 8:00 AM subside by 130 mb over 40 hours, or 0.9 cm/s. Prior to 8:00 AM, the entrainment rate is 0.7 cm/s as calculated using the ozone/flux jump method. In the early morning we expect that the inversion height will rise because the entrainment rate is faster than the subsidence rate. Later in the morning, the entrainment rate lowers to 0.1 cm/s, which is significantly lower than the subsidence rate. We expect the boundary layer depth to decrease in this region as is apparent from the lower inversion height and cloud break-up.

5.3 SATELLITE IMAGES

A series of visible and infrared satellite images as well as maps of 1000 mb geopo-

tential height and wind fields indicate the synoptic environment during and preceding ASTEX. These images, combined with four day back trajectories, suggest that FT air from June 10 originated in a band of convective clouds. Four days prior to observation, the FT air mass moved northeastward with the convective system very rapidly before following a ridge between low and high pressure regions southeastward into the ASTEX region. The MBL air originated north and east of the convective band and then followed an anticyclonic path around a high pressure system into the ASTEX region. On June 10, the ASTEX region is in a surface high pressure region. The satellite images indicate that FT air was influenced by convective clouds four days prior to observation but otherwise the air experienced no significant weather systems; MBL air experienced only high pressure regimes.

5.4 FLIGHT SUMMARY

On June 10, the flight plan consisted of parallel flight legs at various elevations as summarized in Figure 5.6 and Table 5.1. From this flight plan and the information in the

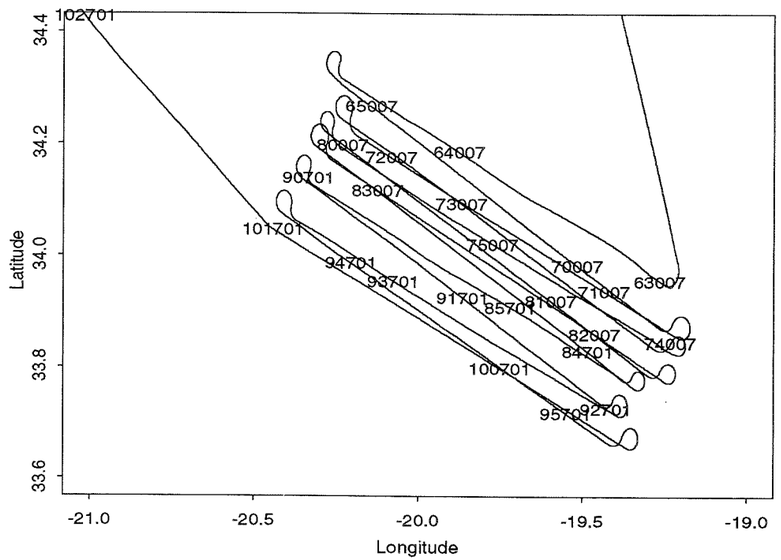

Figure 5.6 Map of June 10 flight path. Times indicated on flight legs.

Table 5.1: Flight segments, June 10, 1992

Time (GMT)	Pressure (mb)	Comment
10:34:00-11:27:10	715	Ferry leg in FT
5:20:00-5:50:00	735	Ferry leg in FT
10:01:57-10:16:49	776	FT
8:17:54-8:32:08	797	FT
7:59:33-8:14:38	859	In cloud
9:43:48-9:59:01	860	In cloud
7:41:50-7:57:00	872	In cloud
9:27:00-9:41:30	875	In cloud
7:24:01-7:39:15	893	MBL
7:07:08-7:21:40	920	MBL
6:48:55-7:04:00	954	MBL
9:09:02-9:24:08	954	MBL
6:30:48-6:45:34	1022	Sea surface
8:51:25-9:06:28	1022	Sea surface

preceding sections, it is evident that the flight legs were flown primarily perpendicular to the prevailing wind. It is also evident that very few measurements are available in the FT, and a significant portion of the data set is unusable for particle analyses due to in cloud instrumentation errors.

5.5 MBL: JUNE 10, 1992

In this section I will discuss particle processes in the MBL in an attempt to understand which processes control the observed particle properties in the MBL on June 10.

5.5.1 Sea salt source

As mentioned in Section 2.1.8 and Section 4.5, sea salt particles in the atmosphere are produced by winds blowing over the ocean surface. In order to assess the portion of the refractory particle population which is sea salt, I complete the analysis outlined in Section 4.5. From this analysis, I find the correlation between mean horizontal particle flux ($\overline{u}\,\overline{RCN}$) and turbulent vertical particle flux ($\overline{w'RCN'}$). I plot these correlations as a func-

tion of minimum horizontal wind speed, in order to see the dependence of the correlation function on wind speed. These results are plotted in Figure 5.7 and illustrate that RCN

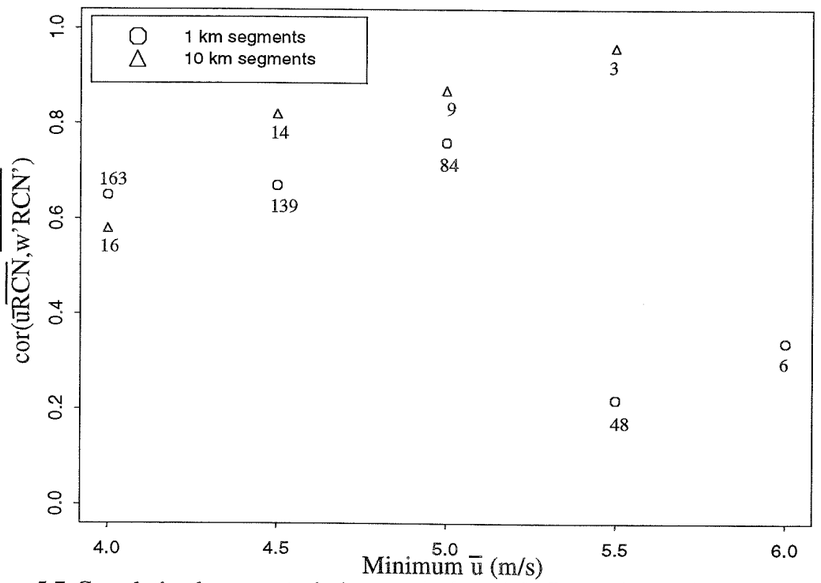

Figure 5.7 Correlation between turbulent vertical particle flux and mean horizontal particle flux for wind speeds greater than a minimum value. This plot indicates that RCN concentrations are correlated with wind speed and thus we can assume that RCN are composed of sea salt. Numbers on plot indicate number of points used in correlation.

turbulent vertical fluxes are approximately 80% correlated with mean horizontal RCN fluxes. The correlation increases with wind speed as expected for sea salt until the number of data points fall off and decrease the correlation due to insufficient sampling, except for the 1 km point at 5.5 m/s which falls off for some unknown reason. These results suggest that the RCN concentrations at the lowest sampled elevation (~50 m) have a surface source and thus that they are largely composed of sea salts.

The strength of the sea salt source and other sea salt source and sink processes will be discussed in terms of RCN transport in the following sections.

5.5.2 Transport in the MBL

I will discuss horizontal transport in terms of characteristic times for transport across a 60 km flight segment. I will discuss vertical transport by an examination of mean and turbulent particle fluxes. The difference in presentation for the two cases is due to the relative importance and variability of the two processes.

- ***Horizontal transport***

Mean horizontal transport times indicate the rapidity with which particles are transported from one region to another as represented by Equation 4-6. Average characteristic times for mean horizontal transport of particles in the MBL along a 60 km flight segment are on the order of 10 hours for all particles. The direction of transport is always downwind. In the case of flight segments which are apparently crosswind, there is usually still some downwind component in the wind parallel to the flight segment which determines the direction of transport. VCN transport times are slower than UCN times which are slower than RCN times. This may indicate that ultrafine particles have both a refractory and a volatile component with characteristics of each component. Since particle concentrations are relatively uniform in the MBL on June 10, mean horizontal transport has little effect on particle concentrations.

- ***Vertical transport***

The vertically-stacked flight legs during ASTEX enable us to calculate transport times for both mean and turbulent motions in the vertical direction between flight legs (see Section 4.4.4). All vertical UCN transport times on June 10 are NA due to logical inconsistencies in the particle data set. Since transport times are obtained from the flux gradients, I will discuss the vertical variability of vertical particle fluxes in order to assess particle sources and sinks. Vertical mean and turbulent fluxes for VCN and RCN below cloud are listed in Table 5.5, delineated by pressure. Negative fluxes are indicative of downward motion and positive fluxes of upward motion.

- ***Mean vertical transport***

Mean particle fluxes (VCN and RCN) in the MBL become increasingly negative toward the sea surface. This is due to increased mean vertical wind speeds in the flight segments at 60 m elevation. Vertical velocities should approach zero near the sea surface,

Table 5.2: MBL vertical fluxes, June 10

Time (GMT)	Pressure (mb)	$\overline{w}\,\overline{n}$ (#/cm^2/s) *(highly uncertain)*		$\overline{w'n'}$ (#/cm^2/s) lo: L > 10 km; hi: L < 10 km			
		RCN	VCN	RCN lo	RCN hi	VCN lo	VCN hi
7:07:08	920	-1430	-570	-290	-70	-60	+10
6:48:55	954	-1950	-800	-165	-120	-15	-3
9:09:02	955	-1310	-645	-100	+30	-45	-36
6:30:48	1022	-2470	-1370	-15	-35	-5	+3
8:51:25	1022	-2450	-1340	+20	+10	+10	+8

so this trend is likely erroneous.

The refractory particle fluxes are larger than the volatile particle fluxes throughout the MBL. Since the winds used for the RCN and VCN flux calculations are the same , the difference in mean flux magnitudes is indicative of RCN concentrations which are higher than VCN concentrations throughout the MBL. This is expected from particle soundings (Figure 5.3).

- ***Turbulent vertical transport***

Turbulent vertical fluxes in the MBL are variable in direction and magnitude which one might expect in a MBL which is undergoing some mixing. The RCN fluxes are larger than the VCN fluxes. This trend indicates that the RCN concentrations are more variable than the VCN concentrations.

The low frequency flux components are larger than the high frequency components for both RCN and VCN. This indicates that the fluxes acting on length scales longer than 10 km dominate the turbulent flux.

Turbulent flux magnitudes decrease toward the sea surface. In the case of refractory particles, this may be due to sporadic injections of sea salt particles. This would create regions of positive w'N' which, when averaged over the entire flight leg, would balance the negative w'N' which dominates above, thus decreasing the turbulent flux. This trend exists in the volatile particle component as well, implying that there is a surface source of volatile as well as of refractory particles. It is possible that this volatile source is

due to low level constant nucleation as conjectured by Coffman and Hegg (1995). Another possible volatile and refractory source is direct emission of organic particles from the sea surface.

One surface flight leg (8:51) has positive turbulent fluxes for both volatile and refractory particles. This is indicative of a surface source of particles which one would expect to be sea salt and hence refractory. This is also further evidence of a volatile particle surface source such as organic particles.

We can demonstrate the importance of vertical transport by analyzing an observed decrease in refractory particle concentration over a 4 hour period on June 10. During a

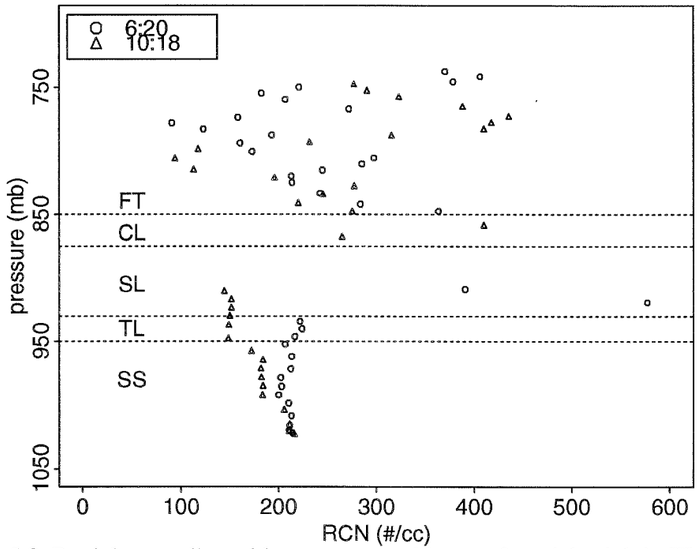

Figure 5.8 Particle soundings 4 hours apart: evidence of particle sink in TL/SL. Particle concentrations at 10:18 have decreased in the transitional layer due to mean vertical transport of particles toward the surface layer.

period in late morning, the particle concentration in the SL and TL regions falls off from its previously constant value (see Figure 5.8). Time scale and flux analysis of this situation indicate that the only particle sink for which we have reliable measurements in this

region is turbulent vertical transport of particles downward, out of the SL and TL layers. Turbulent vertical particle flux is decreasingly negative as altitude decreases so, as time passes, particle concentrations decrease in the TL and SL layers, as shown in Figure 5.8. Interestingly, there is no observed increase in refractory concentrations in the SS layer due to this transport. This must be due to a sink which balances the source from the TL/SL region. Over the four observed hours, there is apparently no particle source to replenish the particle concentration in the TL and SL layers, nor is mixing strong enough to counter the effect of the vertical transport. Further discussion of budgets such as this one will ensue in Chapter 8.

The conclusions which we can draw regarding vertical particle transport in the MBL are:

1. Mean vertical transport is inconclusive due to instrument inaccuracy.

2. Turbulent mixing acts as a source of refractory and volatile particles in the middle MBL.

3. Turbulent mixing at the surface serves as a source of both refractory and volatile particles in the MBL, but this source is not strong. The refractory source is likely sea salt, the volatile source is possibly low level nucleation or organice emissions from the sea surface.

4. There is evidence of small scale turbulent mixing although larger scale mixing is more dominant.

- ***Cross inversion transport***

Finally, we are interested in assessing transport across the inversion. This is accomplished using Equation 4-5. The entrainment rate on June 10 is 0.7 cm/s prior to 8:00 AM, and 0.1 cm/s after 8:00 AM. Therefore we will have two calculations for particle flux into the MBL due to entrainment. The results of this calculation (Table 5.3) indicate that volatile particles will be entrained into the MBL consistently, but this term is not nearly as large as the mean vertical transport terms. RCN and UCN are also entrained but not as rapidly as the VCN. The fact that the entrainment flux term is small further intensifies the need for a particle source in the upper MBL as discussed above in regards to the

Table 5.3: Particle flux due to entrainment
Note: negative fluxes indicate incorporation of FT particles into the MBL.

Time	w_e (cm/s)	$w_e(n_{CT} - n_{BL})$ (#/cm^2/s)		
		RCN	VCN	UCN
Before 8 AM	0.7	+30	-50	-10
After 8 AM	0.1	-11	-30	-1

vertical flux terms. In one case, the RCN is apparently *de*trained due to the fact that there are fewer RCN above the inversion than below.

5.6 FREE TROPOSPHERE: JUNE 10, 1992

5.6.1 Transport in the Free Troposphere

- ***Horizontal transport***

We can summarize horizontal transport times across a 60 km flight segment as follows:

1. UCN horizontal transport times are faster than VCN or RCN transport times in the FT. Since the winds used for all particle fluxes are the same, this difference is due to the fact that the gradients in ultrafine particle concentrations is greater than that for refractory or volatile particles.

2. In the majority of cases, transport times are on the order of 10 - 20 hours.

3. UCN and VCN transport times are less than 1 hour across the boundary of an elevated concentration zone (ECZ) in which UCN and VCN concentrations are elevated relative to the surroundings, but RCN concentrations are not (5:37 GMT). RCN transport times are about 26 hours in this elevated concentration zone (ECZ). The difference in UCN/VCN times and RCN times is expected because the particle gradient is large across the ECZ boundary for UCN and VCN, but not for RCN.

4. Vertical delineation of averaged horizontal transport times are presented in Table 5.4.

5. UCN and VCN transport times (not including ECZ influence) are fastest just above cloud at pressures between 800 mb and 860 mb and slower above and below this region.

neous. The nature of the refractory upper FT source is unclear. Perhaps there is transport of dust into this region. Because the flux magnitudes are relatively constant in the FT, we can stipulate that the particle source is relatively constant.

I would like to illustrate what the effect of an offset in vertical velocity might have on the profile of refractory particle fluxes mentioned in the previous paragraph (see Figure 5.9). The offset would produce zero velocities (and hence fluxes) at the surface and in the

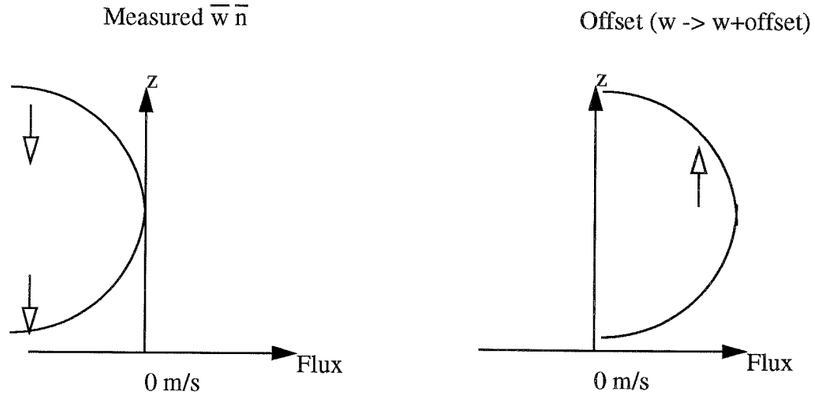

Figure 5.9 Schematic illustrating effect of applying an offset in vertical velocity. Arrows with open heads illustrate the direction of particle transport due to flux gradients.

upper FT and positive mean fluxes in between. This would imply that the MBL and the cloud are serving as a particle source for the FT. This is not probable for the observed environment on June 10 during which the particle concentrations above cloud are higher than those below cloud. This type of schematic illustrates that the vertical velocities are likely negative, despite occasional erroneous regions (such as the sea surface in this case).

For ferry flight legs prior to 11:00 AM, the mean volatile particle fluxes are negative and vary in magnitude. The variability in magnitude is not delineated by height as it is for the refractory particles. This is indicative of the observed episodic bursts in volatile particle concentration. This will show up as bursts in mean particle flux as seen for the

5:30 ferry leg segment which subsumes the 5:37 ECZ.

Ultrafine mean vertical flux values are constant with height, low in magnitude, and negative except for the 5:30 ferry leg which subsumes the 5:37 ECZ. The low fluxes are due to low UCN concentrations throughout the FT except during the 5:37 ECZ. Since there are virtually no ultrafine particles in the MBL, it appears that the UCN have a source in the upper FT and do not reach the MBL. This may be due to diffusional growth or coagulation with other particles which would remove UCN from the ultrafine size range.

- ***Turbulent vertical transport***

Turbulent vertical fluxes are variable in direction for all particles in both the low and high frequency ranges. This is consistent with the expectation that turbulent mixing moves parcels both upward and downward.

Flux values are low and comparable for the low and high frequency ranges for all particles. This suggests that mixing is occurring over both short and long length scales and is not very strong. The FT fluxes are smaller than the MBL fluxes which is indicative of less mixing occurring in the FT than in the MBL.

The total turbulent flux magnitude in the FT appears to be largest at the highest elevations and decrease toward the inversion.

Refractory particle fluxes are positive and volatile particle fluxes are negative at the highest elevations. This is suggestive of air free of refractory particles and full of volatile particles being transported downward. This suggests a source of volatile particles above the region of interest and a source of refractory particles below this region.

The 5:37 ECZ does not act in the same fashion as the other flight segments. This will be discussed in Chapter 7.

Vertical particle fluxes illuminate the following points about transport in the FT.

1. There are volatile and refractory particle sources in the upper FT, but the volatile source seems to be sporadic whereas the refractory source seems to be low in magnitude and constant.

2. Mean transport is downward for volatile and ultrafine particles in all cases. This suggests that particle concentrations are increasing in the middle FT due to upper tro-

pospheric volatile particle sources.

3. Particle transport is directed upward at the inversion. This may indicate the need for a particle source above cloud but also may be due to a combination of instrumentation errors near cloud and inaccuracies in vertical velocities.

4. Vertical turbulent mixing occurs on short and long length scales, but is not strong compared to mean transport.

5.7 Conclusions: June 10, 1992

On June 10 we observe variable particle concentrations in the FT and constant particle concentrations in the MBL. This is expected due to the relatively well-mixed nature of the MBL in contrast to the unmixed FT, especially when coupled with the occurrence of sporadic, large sources in the FT. There is evidence of a surface and free tropospheric source of both refractory and volatile particles. In the sea surface case, the refractory source appears to be larger than the volatile source whereas the opposite is true in the upper FT.

Chapter 6: Case Study, First Lagrangian Mission

In this chapter I will discuss the synoptic, thermodynamic and microphysical environment during the first Lagrangian mission in ASTEX. I will discuss observations and analyze particle processes to the extent that the data set allows.

The first Lagrangian (L1) occurred from June 12-14, 1992. Bretherton and Pincus (1994) and Bretherton, *et. al.* (1994) have discussed the synoptic setting, cloudiness and MBL dynamics for this Lagrangian experiment. Consequently, I will not go into great detail except to reiterate that the boundary layer is relatively well-mixed on these days; the region is not polluted; the inversion height rises during L1 from 970 mb to 920 mb; the cloud deck is solid; and drizzle is occurring on and off throughout these days.

6.1 Soundings

Soundings from L1 display some of the characteristics of these days. Figure 6.1 displays soundings from each of the three Electra flights during L1. These soundings indicate the evolution of the boundary layer. The inversion height rises and becomes sharper over 36 hours; the MBL becomes more decoupled as times progresses; and, throughout L1, there is a significant amount of structure in the FT as seen from the dew point temperature soundings. There appears to be a change in air mass characteristics at about 800 mb which is consistent with the back trajectory analysis (Section 6.2). The inversion is not as sharp at the beginning of L1 as it is on June 10. This is expected because subsidence is not as strong during L1 as on June 10.

During L1, the MBL was characterized by northerly winds with speeds from 6-12 m/s, in contrast to the FT where the winds were out of the N-NE and wind speed ranged from 8-10 m/s. The median vertical wind speed is -0.03 m/s in the MBL and -0.125 m/s in the FT. The near zero vertical wind speed value in the MBL is indicative of relatively equally amounts of upward and downward vertical motion in the MBL. In the FT, on the other hand, motion is consistently downward.

Parallel to the discussion of June 10 (Chapter 5), I have plotted thermodynamic soundings in Figure 6.2 for the three soundings plotted in Figure 6.1. The thermodynamic soundings illustrate that the MBL is very well-mixed on June 12 and becomes progres-

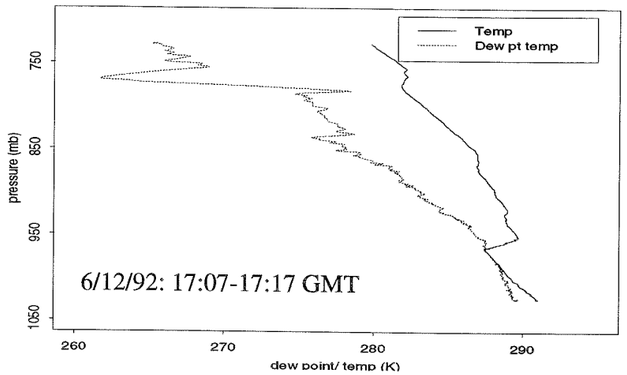

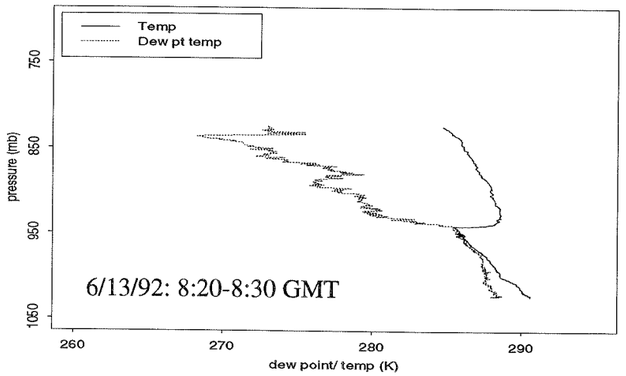

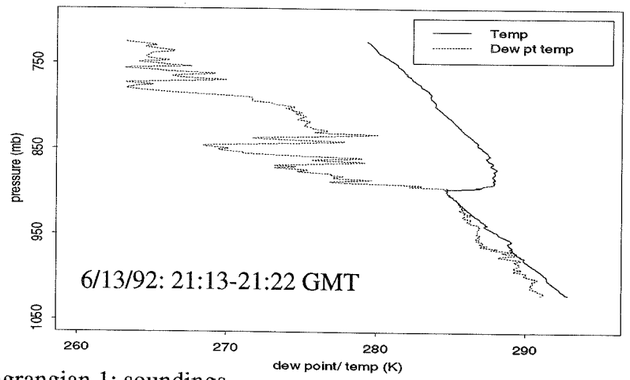

Figure 6.1 Lagrangian 1: soundings.

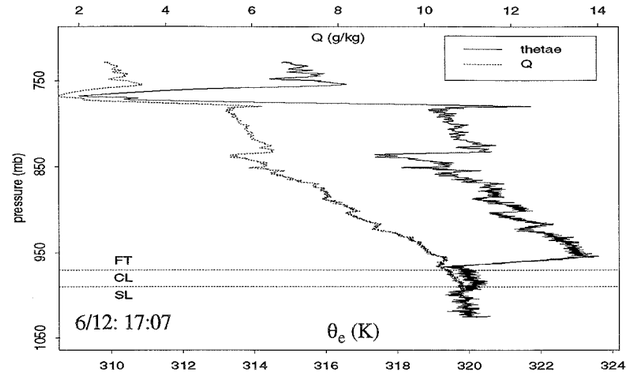

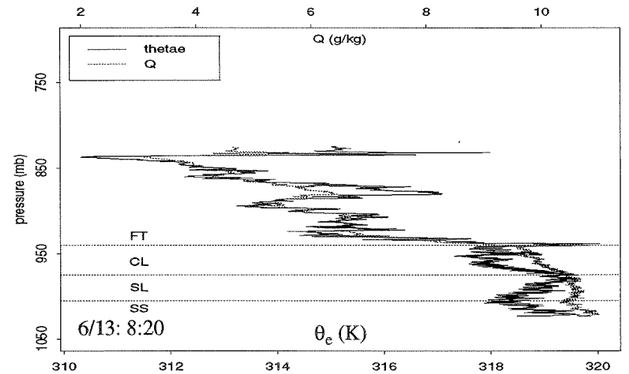

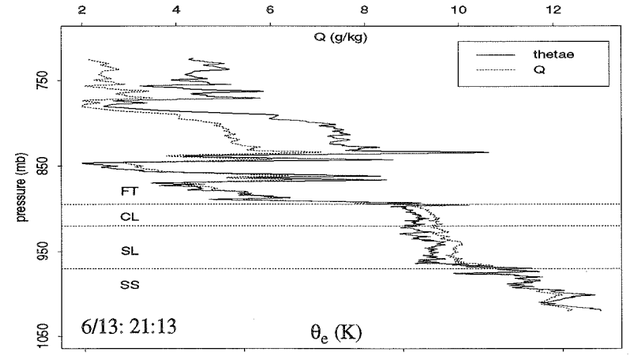

Figure 6.2 Thermodynamic layering during L1. Naming convention for layering is the same as in Figure 5.2.

sively less mixed as the Lagrangian mission continues.

Composite particle soundings for the entire L1 are presented in Figures 6.3, 6.4, and 6.5. The volatile particle concentrations during L1 are relatively low and constant in the MBL and increase with height in the FT (Figure 6.3). Ultrafine CN concentrations fol-

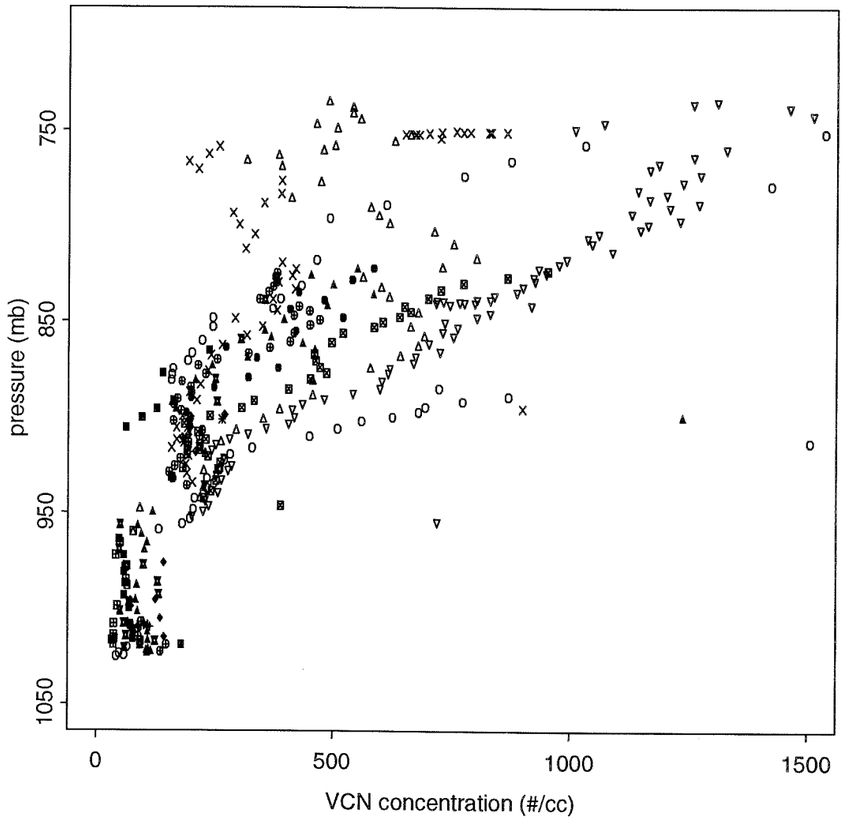

Figure 6.3 Volatile particle soundings during L1: composite of all soundings. The magnitude of the concentration increase with height decreases slightly in time.

low the same trends as VCN (Figure 6.4) and UCN and VCN are frequently correlated. These trends suggest that VCN and UCN have similar sources and sinks. The fact that the highest particle concentrations occur at the top of the FT and are primarily composed of volatile material suggests that a volatile particle source is present at or above this level.

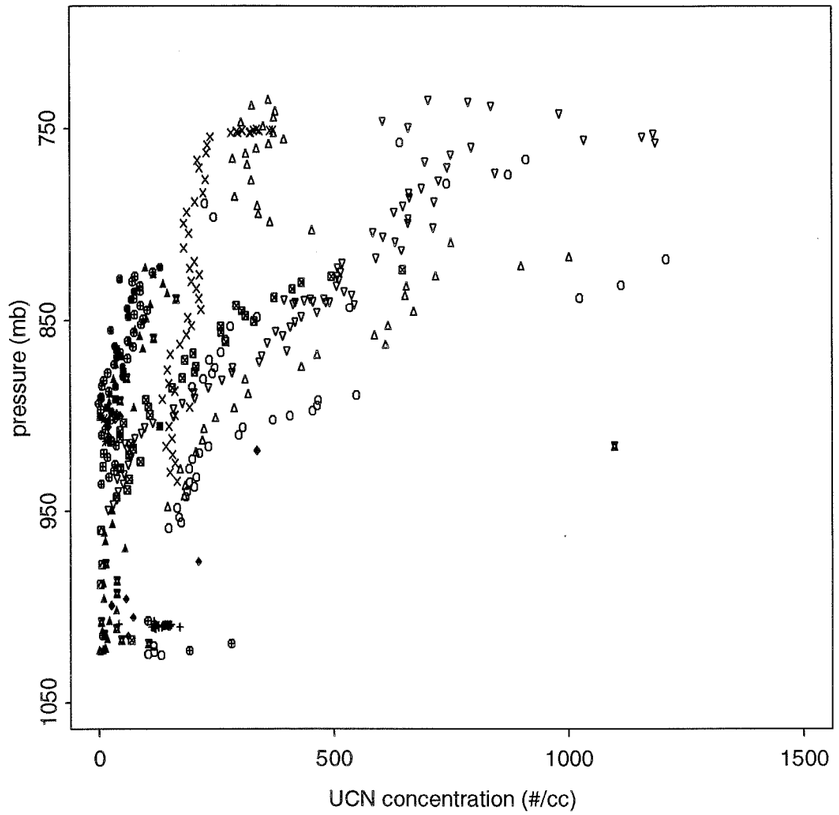

Figure 6.4 Ultrafine particle concentrations during L1. The magnitude of the particle concentration increase with height decreases in time.

There is a jump in volatile particle concentrations across the inversion, from concentrations above the inversion of about 300/cc to concentrations below of about 100/cc. This indicates that there are probably particle sinks in this region, such as clouds or cloud top divergence.

The surface-derived (RCN) component of the particle population in the FT is small and relatively uniform near 100/cc (Figure 6.5). In the MBL, the RCN concentration increases toward the sea surface. The constancy of the RCN concentration throughout most of the atmosphere indicates that refractory particle sources and sinks are in a steady

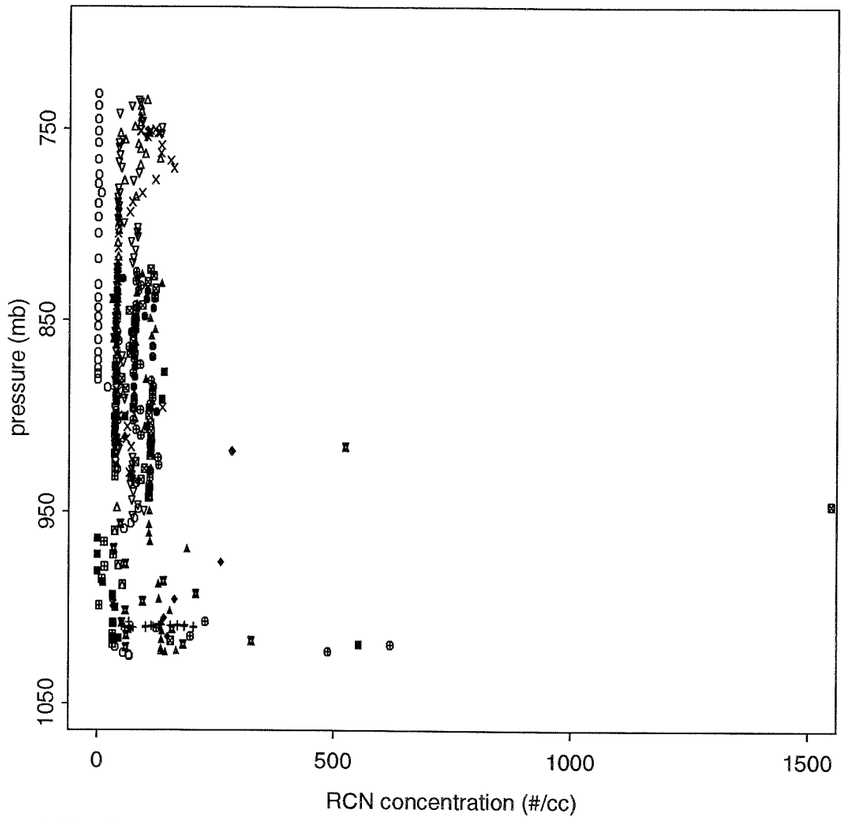

Figure 6.5 Refractory (surface-derived) particle concentrations during L1.

state. The increase in RCN concentration near the surface is likely due to a source of sea salt particles.

As was true for June 10, particle concentrations display little of the boundary layer structure evident in thermodynamic tracers.

6.2 BACK TRAJECTORIES

Back trajectories for various times and elevations during the first Lagrangian mission show that air of two origins is present (Figure 6.6). At elevations above 800 mb, the trajectory tracks back toward Cape Cod. After four days, the air is about 10 degrees east of Cape Cod. For elevations below 800 mb, the air parcels trace an anti-cyclonic path,

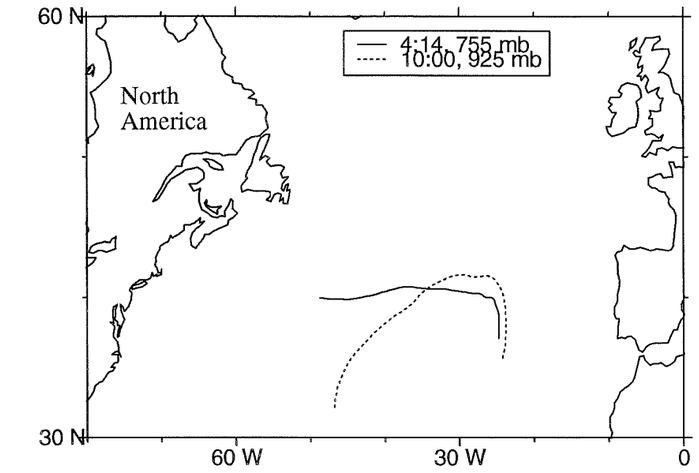

Figure 6.6 Back trajectory from two starting points on 6/13/92. These trajectories are representative of trajectories thoughout L1. Notice different origins for air from different starting elevations.

originating a few degrees south and 20 degrees west of the ASTEX region. The trajectories suggest that none of the air in the ASTEX region during the first Lagrangian had had any continental influence over the four days prior to L1. Although it is possible that the upper free troposphere experienced some northeast U.S. influence, there is no evidence of this in black carbon data once the air reaches the ASTEX region.

The L1 back trajectories display consistent, rather slow subsidence over the four days prior to the first Lagrangian mission. The air parcels subside by about 100 mb over 2.5 days. This translates to a subsidence rate of about 0.5 cm/s (400 m/day) which is approximately the same as Bretherton *et. al.*'s (1994) estimate of the entrainment rate (0.7 +/- 0.3 cm/s). The fact that the boundary layer is deepening throughout L1 suggests that the subsidence rate is slower than the entrainment rate. Both subsidence and large-scale transport are quite a bit slower for the days prior to the Lagrangian mission than those prior to June 10.

6.3 SATELLITE IMAGES

Satellite images and pressure and wind fields during the four days preceding L1 indicate that the air has consistently been moving in anticyclonic motion around a large high pressure system near the ASTEX region. The air mass stays in front of a large convective system throughout this time period. This air has experienced no active weather systems.

6.4 FLIGHT SUMMARIES

The Electra aircraft flew three flights during the first Lagrangian mission. In all three flights crosswind and downwind flight segments were flown. The flight plans and flight segment information are contained in Figure 6.7 and Table 6.1. In Table 6.1 I include only those flight segments for which there is enough particle data to complete the transport analysis. There are many flight segments that we are not able to analyze due to instrument error in and around cloud. These additional flight segments are listed in Bluth and Albrecht (1993b).

6.5 MBL: FIRST LAGRANGIAN MISSION

During L1, the particle concentrations in the MBL are quite constant and are significantly lower than the concentrations in the FT (Figure 6.3-6.5). Of the MBL CN concentration, more than half is surface-derived (RCN) for the MBL as a whole, but this percentage increases slightly toward the surface (Table 6.2). The increase in refractory particle concentrations toward the surface suggests that there is a surface source of sea-salt in the MBL during the first Lagrangian mission. The magnitude of this source and the factors which control it will be discussed in the following section.

6.5.1 Sea salt source

Using the same analysis as is presented in Section 5.5.1, I find that RCN turbulent vertical fluxes are only 50% correlated with mean horizontal RCN fluxes. This is significantly lower than the 80% noted on June 10. This is counterintuitive since the horizontal wind speeds near the surface on June 10 are significantly lower than during L1, as is apparent in the scales on the horizontal axes of Figure 5.7 and 6.8. The apparent difference between June 10 and L1 may be due to the fact that the MBL is more well-mixed on

June 12, 1992

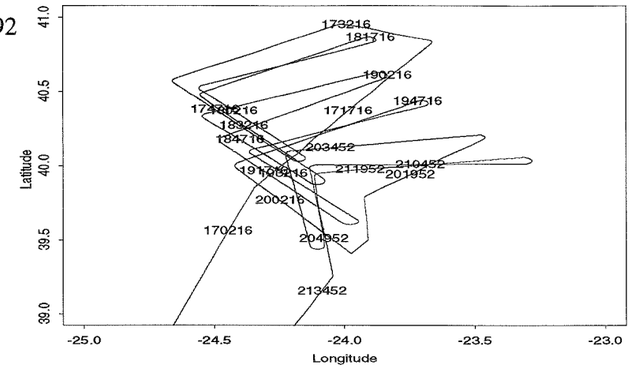

June 13 (1)

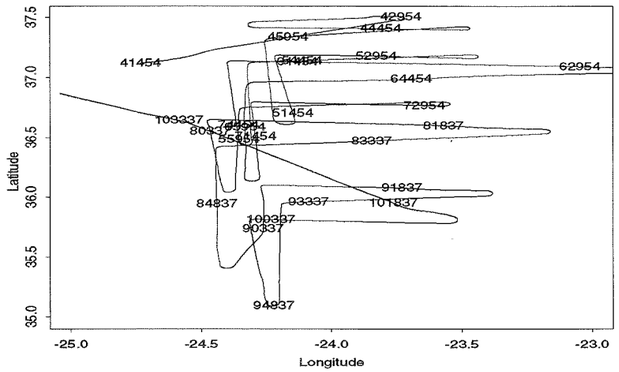

June 13 (2)

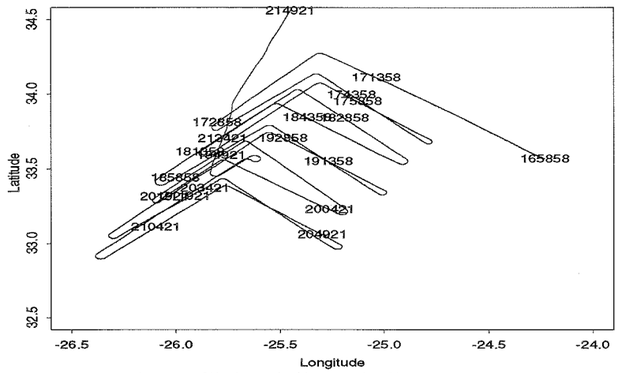

Figure 6.7 Maps of three Electra flights during L1. GMT times are indicated on flight segments.

Table 6.1: Flight segments, June 12/13, 1992
These flight segments are those which have sufficient particle data to be analyzed.

Date	Time (GMT)	Pressure (mb)	Comment
6/12/92	19:58:35-20:08:36	810	FT
6/12/92	19:47:35-19:57:44	821	FT
6/12/92	18:17:44-18:27:51	996	MBL
6/12/92	18:06:12-18:16:14	1010	MBL
6/12/92	20:20:56-20:36:56	1016	MBL
6/12/92	20:37:41-20:47:42	1026	MBL
6/13/92 (1)	4:15:00-4:25:00	737	Ferry leg
6/13/92 (1)	6:00:55-6:10:56	820	FT
6/13/92 (1)	6:11:35-6:22:10	820	FT
6/13/92 (1)	8:31:00-8:41:00	827	FT
6/13/92 (1)	8:41:50-8:52:00	827	FT
6/13/92 (1)	9:51:55-10:01:55	921	FT
6/13/92 (1)	10:03:00-10:13:04	929	FT
6/13/92 (1)	6:54:13-7:04:13	1017	MBL
6/13/92 (1)	9:10:50-9:21:00	1023	MBL
6/13/92 (1)	8:57:50-9:10:14	1024	MBL
6/13/92 (2)	18:46:50-18:56:54	792	FT
6/13/92 (2)	19:52:23-20:02:25	991	MBL
6/13/92 (2)	17:07:10-17:18:36	1022	MBL
6/13/92 (2)	19:30:30-19:40:35	1023	MBL
6/13/92 (2)	17:19:16-17:29:17	1023	MBL

Table 6.2: Portion of MBL particle population which is surface derived

Height	RCN concentration (surface-derived)	VCN concentration (volatile, CN - RCN)	Percentage RCN/CN
950-1000 mb	130/cc	110/cc	54%
1000-1050 mb	135/cc	102/cc	57%

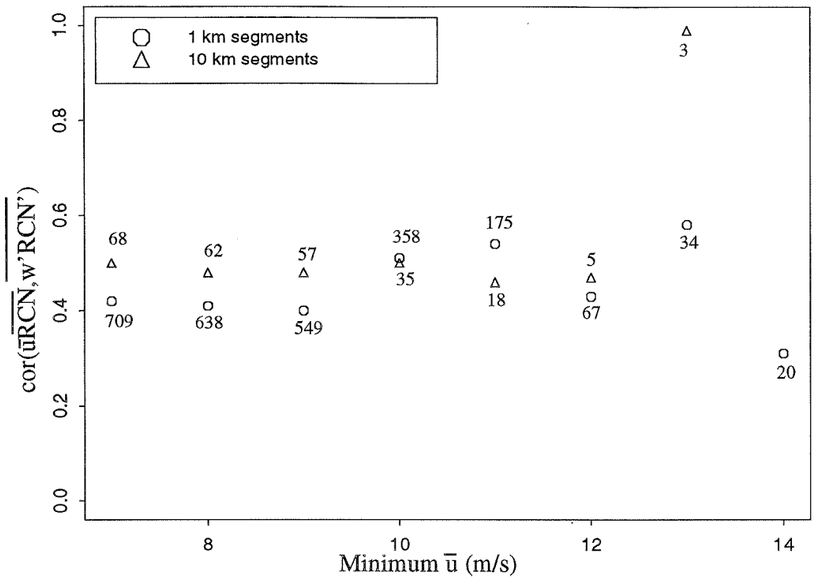

Figure 6.8 Correlation between turbulent vertical particle flux and mean horizontal particle flux. Correlation is plotted as a function of wind speed greater than a designated minimum value. Numbers indicate number of data points used in correlation.

L1. This would serve to dilute the sea salt source, incorporating the salt rapidly into the rest of the MBL. Thus we would not expect to see the effect of the salt source except right near the surface but the lowest flight segments during L1 were flown at 50 m elevation so perhaps we cannot see this effect. Since there is some evidence of a sea salt source (i.e., 50 % correlation between vertical mixing and mean horizontal fluxes), I will speak of refractory particles in the MBL as being sea salt.

6.5.2 Transport in the MBL

I will discuss transport in the same fashion as for the June 10 case study. I will discuss horizontal transport in terms of characteristic times and vertical transport in terms of fluxes. Since this is a Lagrangian mission, I only calculate horizontal transport for approximately crosswind flight segments during which the aircraft is in an approximate Eulerian reference frame.

- ***Horizontal transport***

Average horizontal transport times across 60 km flight segments for all particles in the MBL are on the order of 10 hours. UCN times are the fastest, followed by VCN and RCN which are comparable to one another. Since we are in a Lagrangian reference frame, horizontal transport is only significant insofar as the aircraft is moving at a different speed than the air mass, or as the aircraft is flying perpendicular to the prevailing wind. Some of the L1 flight legs are flown crosswind thus suggesting that there is mean particle transport crosswind. The presence of crosswind transport is only due to the fact that the aircraft is rarely absolutely perpendicular to the prevailing wind and therefore there is a component of the prevailing wind parallel to the flight leg.

- ***Vertical transport***

I will discuss vertical transport in terms of particle fluxes (Table 6.3). Vertical transport times (due to flux gradients) will be incorporated into the budget study in Chapter 8.

- ***Mean vertical transport***

In the MBL, mean vertical fluxes are negative for all but one flight segment in which case the magnitude of the flux is very small (9:10:50 GMT).

Unlike June 10, there is not a consistent increase in flux magnitude toward the sea surface. In fact, the fluxes for sea surface legs ($p > 1020$ mb) are significantly lower than in the upper MBL in all but two cases. The surface flux magnitudes are low because the mean vertical velocity is close to zero. This is expected because the mean vertical velocity must go to zero at the sea surface, implying that these measurements of mean vertical fluxes may be robust.

For the two cases where surface fluxes are not low (6/13 (2); 17:07 and 17:19), the refractory particle flux is much larger than either the volatile or ultrafine particle flux. This is due to high refractory particle concentrations near the surface combined with large, negative mean vertical velocities. This scenario is similar to that on June 10 and is possibly erroneous.

On June 12, ultrafine and refractory particle fluxes in the MBL are comparable to one another and larger than volatile particle fluxes suggesting that the RCN and UCN have

Table 6.3: MBL vertical fluxes, L1

Time (GMT)	Pres. (mb)	$\overline{w}\,\overline{n}$ (#/cm^2/s) *(highly uncertain)*			$\overline{w'n'}$ (#/cm^2/s) lo: L > 10 km; hi: L < 10 km					
		RCN	VCN	UCN	RCN lo	RCN hi	VCN lo	VCN hi	UCN lo	UCN hi
June 12, 1992										
18:17:44	996	-1426	-1107	-1538	-4	2	-6	-2	4	0
18:06:12	1010	-1674	-1371	-2008	-1	0	1	-7	3	-21
20:20:56	1020	-2146	-1404	-1963	-121	9	-3	-14	-55	-37
20:37:41	1026	-449	-295	-460	26	24	-12	2	0	14
June 13, 1992 (1)										
6:54:13	1017	-3135	-1720	-1253	68	318	-3	23	111	143
9:10:50	1023	37	18	8	136	139	24	31	33	37
8:57:50	1024	-198	-84	NA	431	80	89	10	NA	NA
June 13, 1992 (2)										
19:52:23	991	-586	-587	-206	-55	-31	-53	1	-42	67
17:07:10	1022	-1469	-769	-369	293	-4	19	-5	174	-3
19:30:30	1023	-200	-130	-82	171	-1	0	7	71	84
17:19:16	1023	-1175	-703	-150	-3	5	7	-7	-4	-3

similar sources and sinks. It is possible that sea salt particles are being observed in the ultrafine size range although this has never been previously observed.

On June 13, the refractory particle fluxes are larger than volatile particle fluxes which are larger than ultrafine particle fluxes. This is due to increased refractory particle concentrations and decreased ultrafine particle concentrations on June 13 relative to June 12 which suggests a refractory particle source and an ultrafine particle sink on June 13. Wind speeds are higher on June 13 than June 12 which suggests a larger sea salt source which might explain increased RCN concentrations. UCN concentrations, in general, will decrease in time without a persistent source due to processes such as coagulation and gaseous deposition which serve to move ultrafine particles into the CN size range. Therefore, lower UCN concentrations on June 13 may only indicate that there is no longer an

ultrafine particle source to resupply those UCN which have grown into the CN size range.

- ***Turbulent vertical transport***

Turbulent vertical fluxes vary in direction for all particles throughout L1. This is expected for a relatively well-mixed region.

Low and high frequency components of the turbulent flux are comparable in magnitude for all particles for most flight segments. Occassionally the low and high frequency flux components are opposite in direction. This suggests that there are significant differences in mixing on various length scales. Of course, when low and high frequency fluxes are comparable in magnitude and opposite in direction, the overall turbulent flux is close to zero.

Turbulent vertical fluxes are consistently low for volatile particles. This suggests that there are no significant volatile particle sources or sinks due to turbulent mixing or that no sources or sinks are apparent due to the fact that the MBL is well mixed with respect to volatile particles.

Refractory turbulent fluxes are large and positive during most of June 13. This is consistent with the implication from mean flux calculations that there are sporadic refractory particle sources, such as sporadic sea salt production, in the MBL.

Vertical transport in the MBL can be summarized as follows:

1. The well mixed nature of the MBL during most of L1 serves to decrease the variability in flux magnitudes. This limits my ability to draw conclusions about source and sink terms from particle fluxes in the MBL.

2. Mean and turbulent fluxes indicate that there are refractory particle sources on June 13 which are likely sea salt.

- ***Cross inversion transport***

Transport of particles into the MBL due to entrainment at cloud top is presented in terms of particle fluxes in Table 6.4. As in the June 10 case, the entrained particle flux is low compared to the fluxes due to mean vertical winds within the MBL. A particle source other than entrainment in the upper MBL is necessary to maintain the negative particle fluxes within the MBL. The volatile particle entrainment fluxes are highest due to the fact

Table 6.4: Particle flux due to entrainment

Date	w_e (cm/s)	$w_e(n_{CT} - n_{BL})$ (#/cm^2/s) (-): source for MBL		
		RCN	VCN	UCN
June 12, 1992	0.7	-105	-210	-35
June 13, 1992 (1)	0.7	-110	-150	-50
June 13, 1992 (2)	0.7	-90	-200	-20

that there is the largest gradient in volatile particle concentration across the inversion.

6.6 FREE TROPOSPHERE: FIRST LAGRANGIAN

6.6.1 Transport in the Free Troposphere

- ***Horizontal transport***

We can summarize horizontal transport times across a 60 km flight segment during L1 as follows:

1. Most horizontal transport times are on the order of 10 hours for all particles. This uniformity is likely due to the fact that the gradient in wind speed dominates over the gradient in particle concentration.

2. RCN transport times are longer than UCN and VCN transport times in the FT.

3. UCN and VCN transport times are on the order of 1 hour across the 4:18 ECZ boundary. This is expected because the particle gradient is large across ECZ boundaries, by definition (see Chapter 7 for more discussion).

4. The RCN transport time is longer than UCN and VCN times across the ECZ boundary and is on the order of 10 hours. This is indicative of the fact that the RCN gradient is small across ECZ boundaries.

5. Vertical delineation of average horizontal transport times are presented in Table 6.5.

6. Averaged UCN and VCN transport times are relatively constant throughout the MBL and lower FT. The range of transport times over which I average is wide. This is indicative of the fact that UCN and VCN concentrations are quite variable: in some cases concentrations are constant over large horizontal extents; at times varying by orders of

8/10 E/9

Table 6.5: Horizontal transport times during L1

Pressure range (mb)	Time (hours) VCN	UCN	RCN
700-800 4:18 ECZ:	4.3 1.1	4.7 0.8	12 12
800-900	12	12	14
cloud	NA	NA	NA
>900	14	12	14

magnitude over short distances.

7. The upper FT (700-800 mb) is the only non-ECZ region with average mean horizontal transport times for UCN and VCN which are shorter than 12 hours over 60 km.

8. VCN and UCN transport times are fastest at the highest elevations and slowest in the MBL. RCN transport times are approximately constant throughout the MBL and the FT.

9. The fact that UCN and VCN horizontal transport times are fast aloft is indicative of the observed, sporadic sources of UCN and VCN aloft. The variable UCN concentrations in the FT can cause large particle flux gradients which, in turn, shorten transport times as in the case for the ECZ. The fast transport times across ECZ boundaries suggest that particle concentrations will decrease rapidly in a given region due to mean horizontal transport out of such a region.

- ***Vertical transport***

I will discuss vertical transport in the FT in terms of particle fluxes.

- ***Mean vertical transport***

Mean vertical fluxes in the FT are consistently negative for all particles.

Mean vertical fluxes tend to decrease with decreasing height in the FT. This suggests that the upper FT is a particle source for the lower regions of the FT. Volatile and ultrafine particles are the dominant component of this source. This is consistent with volatile and ultrafine particle soundings which indicate a particle source in the upper FT.

Mean volatile particle fluxes are larger in magnitude than ultrafine particle fluxes

Table 6.6: FT vertical fluxes, L1

Time (GMT)	Pres. (mb)	$\overline{w}\,\overline{n}$ (#/cm^2/s) *(highly uncertain)*			$\overline{w'n'}$ (#/cm^2/s) lo: L > 10 km; hi: L < 10 km					
*= ECZ		RCN	VCN	UCN	RCN lo	RCN hi	VCN lo	VCN hi	UCN lo	UCN hi
June 12, 1992										
19:58:35	811	-243	-3856	-2785	-7	0	-50	-14	71	4
19:47:35	821	-441	-7473	-4704	7	0	457	45	279	35
June 13, 1992 (1)										
4:15:00*	737	-6216	-53284	-87658	1058	410	11007	456	27534	4333
6:00:55	820	-865	-19673	-23979	-13	-1	-297	-56	-2148	-106
6:11:35	820	-550	-13875	-8737	7	-30	-64	17	-58	32
8:31:00	827	-643	-6890	-3994	-57	-4	-250	-29	-308	-5
8:41:50	827	-252	-4081	-2394	-5	-16	6	10	24	-13
9:51:55	921	-365	-2014	-174	0	-1	-3	8	-24	-4
10:03:00	929	-450	-1907	-212	-7	-1	-17	-1	6	4
June 13, 1992(2)										
18:46:50	792	-744	-3366	-723	6	0	24	-4	-2	-12

in all cases except for the flight segment which subsumes the 4:18 ECZ and one other instance. This is likely due to the fact that high UCN concentrations are not long-lived due to growth processes (see Chapter 7) which form VCN.

Mean refractory particle fluxes are low compared to UCN and VCN fluxes and do not vary as much with elevation. This is due to the fact that there is no large source of refractory particles in the upper FT. There is net downward transport of RCN in the FT which does imply that there is a weak refractory particle source in the upper FT.

- ***Turbulent vertical transport***

Turbulent vertical fluxes are variable in direction for all particles throughout the FT.

Turbulent fluxes of refractory particles are low in magnitude except for the 4:18 ECZ. This is due to the fact that refractory concentrations are higher than usual during the

4:18 ECZ.

Turbulent volatile and ultrafine particle fluxes are quite large high in the FT and decrease toward the inversion. Most of the fluxes which are large in magnitude are negative indicating that particles are being mixed downward as well as being transported downward due to mean motions.

For volatile and ultrafine particles, turbulent fluxes are predominantly acting over length scales larger than 10 km. For refractory particles, low and high frequency components of the turbulent flux are comparable but low in magnitude.

During the 4:18 ECZ turbulent fluxes are positive. This is true for the June 10 5:37 ECZ as well. This will be discussed in Chapter 7.

Vertical transport is summarized in the following statements.

1. Mean motions dominate over turbulent motions in all cases.

2. Mean transport is downward for volatile and ultrafine CN in all cases. This indicates that particle concentrations are increasing in the middle FT due to upper tropospheric particle sources.

3. During L1, turbulent transport is variable in direction and magnitude but, for volatile and ultrafine particles, turbulent transport still serves as a source of particles for the middle and lower FT.

4. Vertical fluxes above the inversion are larger than the entrainment fluxes.

6.7 CONCLUSIONS: FIRST LAGRANGIAN MISSION

During L1 we see strong evidence for a source of volatile particles in the FT. Flux analysis indicates downward transport in the FT, consistent with the proposed source region. There is some evidence of a particle source at the sea surface but the well mixed nature of the MBL makes this source difficult to assess with transport calculations.

The results discussed in this chapter will be incorporated into particle budgets in Chapter 8. The budget study will quantify the cumulative effects of the observed processes and will indicate the necessary strength of processes which are not observable in order to balance the budget.

Chapter 7: Analysis of Elevated Concentration Zones

Observations of particle concentrations during the unpolluted portion of ASTEX lead me to hypothesize that volatile particles are produced in the upper free troposphere and are transported downwards. In this chapter, I will summarize the observations which lead me to this conclusion and then present a detailed analysis supporting my hypothesis.

7.1 ECZ OBSERVATIONS

The most interesting particle behavior in the FT during L1 and June 10 occurs in localized instances when volatile and ultrafine particle concentrations jump dramatically without a corresponding jump in refractory particle concentrations (Figure 7.1). I refer to

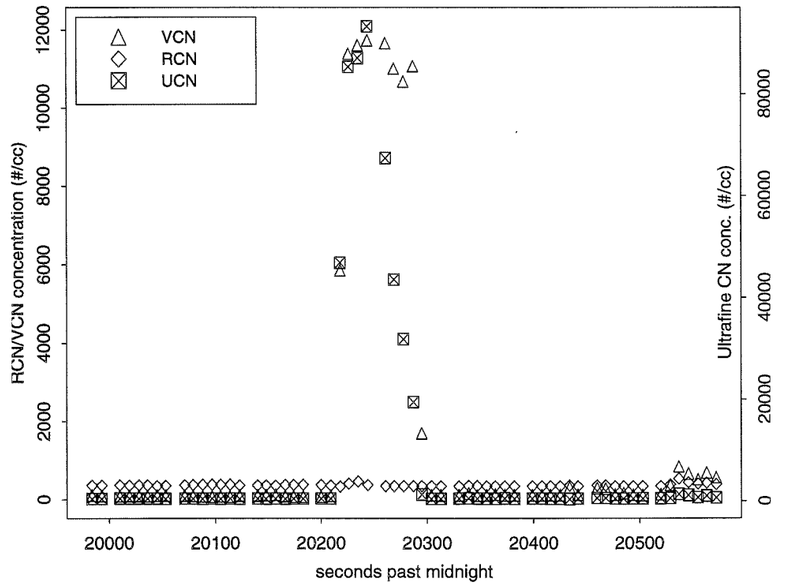

Figure 7.1 5:37 ECZ on June 10, 1992.

these instances as elevated concentration zones (ECZs) and summarize them in Table 7.1 and the following statements.

1. ECZs with total particle concentration greater than 10,000/cc (6/10 5:37; 6/13

Table 7.1: ECZs in Free Troposphere

Time (GMT)	Date	Magnitude (#/cc)	Height	Extent* (* see #2 below)	Mean vert. wind
5:37-5:38:07 (see Figure 7.1)	6/10/92	VCN: 12000 UCN: 4850-43000 RCN: 360	2630 m	14 km	- 0.15 m/s
16:45-17:06	6/12/92	VCN: 2500-5000 UCN: 2000-4200 RCN: 200	2736 m	158 km	- 0.13 m/s
21:56-21:59	6/12/92	VCN: 2525-3350 UCN: 1780-2280 RCN: 45	2432 m	17 km	- 0.08 m/s
4:18:50-4:20:40 (see Figure 7.2)	6/13/92 (1)	VCN: 6800-11700 UCN: 12700-41900 RCN: 90	2606 m	15 km	- 0.13 m/s
8:32:47-8:34:05	6/13/92 (1)	VCN: 600-1500 UCN: 250-970 RCN: 80-215	1680 m	21 km	- 0.15 m/s
10:20-10:35	6/13/92 (1)	VCN: 2050-2350 UCN: 900-1600 RCN: 40	2302 m	95 km	- 0.1 to + 0.1 mean: - 0.02

4:18) are at some of the highest elevations (> 2600 m) sampled by the Electra.

2. The two ECZs with highest concentrations (6/10 5:37; 6/13 4:18) are small in horizontal extent, as measured by aircraft which sample only one cross-section of a three dimensional ECZ. Both large ECZs are observed in crosswind flight segments. It is possible that the ECZ is elongated downwind which implies that we are observing the smallest dimension of the ECZ.

3. ECZs are predominantly composed of volatile particles. In the unpolluted marine environment, sulfate is the dominant component of volatile particles. This implies that the ECZs are primarily composed of sulfates.

4. Very large downward mean particle fluxes exist for all ECZs, and hence very short downward transport times (see Section 5.6.1 and Section 6.6.1). Turbulent vertical transport is directed upward for the two ECZs with highest concentrations but these fluxes

are not large enough to offset the effect of the mean transport.

5. The ECZs with highest concentrations are observed very early in the morning GMT time - before sunrise local time.

6. The ECZs with highest concentrations consist primarily of UCN, i.e., particles with diameter between 3 and 15 nm.

7. ECZs with total particle concentrations less than 10,000/cc have comparable numbers of UCN and VCN.

These observations, along with the following analysis of the various source and sink processes which particles might undergo, lead me to conjecture that nucleation high in the troposphere is producing high concentrations of small volatile particles which are then transported downward. During transport, the particle size distribution shifts to larger particles in smaller concentrations due to particle processing, namely coagulation. Discussion of the analysis of these ECZs and the evidence in support of my hypothesis constitute the following sections.

7.2 Mass conservation

Prior to a detailed analysis of particle processing, it is interesting to assess the contribution of ECZs to the total particulate loading of the lower atmosphere. A simple mass conservation analysis can illustrate the plausibility of the suggestion that ECZs contribute significantly to the particle concentration just above the inversion layer. The assumptions which I use for this estimate are:

1. All UCN have 5 nm radii.

2. All VCN have 15 nm radii (from C131-A DMPS size distributions taken on 6/13/92 at 1300 m and 600 m altitude).

3. All particles have the same mass density.

4. ECZs have a circular cross-section, with the diameter determined by the flight path through the ECZ.

5. There is a uniform layer of volatile and ultrafine particles above the inversion over the entire flight region, i.e., 2° latitude by 1.5° longitude or 222 km by 137 km. This assumption is based on observations.

6. Particle concentration at the inversion layer is constant over the entire flight region at approximately 200 VCN/cc and 100 UCN/cc.

Using all of these assumptions, I find that we would need 2.5 ECZs of the same size as the 4:18 ECZ on 6/13/92 to provide the mass that exists in the observed particle layer above the inversion. This displays the significance of observed ECZs in the overall particle budget in the remote marine environment.

7.3 ECZ ANALYSIS

Observations suggest that ECZs are due to nucleation products which have undergone evolution due to particle processing. I would like to illustrate this more definitively through the analysis of particle processes such as coagulation, particle growth due to deposition of gases, transport, and nucleation itself. This analysis requires an inverse approach because the observations are of particles that have already undergone processing. My goal is to determine the concentrations of newly nucleated particles that could evolve into the observed concentrations via particle processing.

7.3.1 Coagulation results

I will examine forward and backward evolution of the 4:18 ECZ on 6/13/92 as an illustration of the role that coagulation may play in transforming newly nucleated particles into those observed in an ECZ, and then transforming the observed ECZ particles into those typical of the FT.

Information about particle size is necessary for an evaluation of coagulation rates. During the first Lagrangian the only size information available are that the UCN and CN instruments measure over specified size ranges and that size distributions from 0.14-7.0 μm are measured by the laser optical particle counter (OPC).

During the 4:18 ECZ, there are two different modes (see Figure 7.2): one with UCN concentrations of 34,000-40,000/cc and VCN concentrations of 4,000/cc which spans only 2 km (mode I); and the other with UCN concentrations of 16,000/cc and VCN concentrations of 12,000/cc over a distance of 8 km (mode II). I assume that what I am observing in mode I is a monomodal lognormal distribution with a portion of the particle concentration in the CN size range and a portion in the UCN size range (see Figure 7.3).

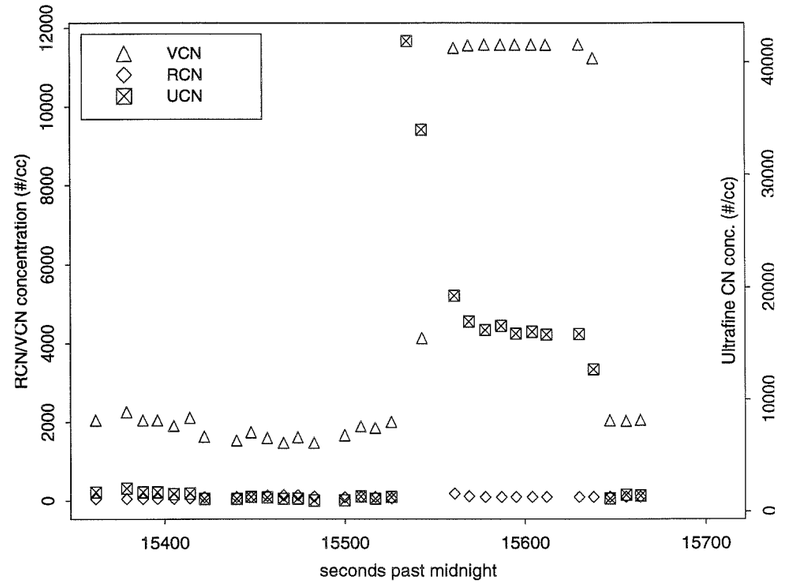

Figure 7.2 4:18 ECZ on 6/13/92. Notice highest peak in UCN just before 15550 (mode I) which then decreases to ~16,000/cc just past 15550 (mode II).

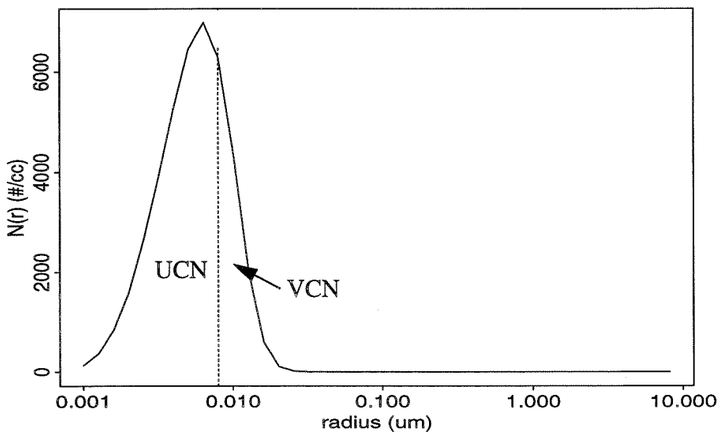

Figure 7.3 Lognormal distribution consistent with observed particle concentrations in mode I of the 4:18 ECZ.

I now ask whether the observed 4:18 ECZ could have formed by coagulation of

newly nucleated particles. The first step in analyzing the 4:18 ECZ is to determine what distribution and initial conditions can produce the observed concentration shown in Figure 7.3 via coagulation. The input parameters which I vary in order to find the appropriate initial conditions are total concentration, distribution standard deviation and single and double lognormal distributions. The assumptions which I keep fixed are: the dominant lognormal curve is peaked at 1 nm radius, indicative of freshly nucleated particles; the mass density is 1.3 g/cc as obtained from D. Coffman's code for freshly nucleated particles; the temperature and pressure are the same as at the 4:18 ECZ, namely, 8° C and 737 mb, respectively. Given these assumptions, I find that the only way coagulation can create the 4:18 ECZ is from a single lognormal distribution with a very high initial concentration and variable distribution standard deviation. The most realistic scenario is an initial concentration of 1.2 x 10^6/cc and a standard deviation of 1.85.

The results of the coagulation analysis for mode I of the 4:18 ECZ for the backward (-) and forward (+) evolution of 34,000 UCN and 4,000 VCN are shown in Table 7.2 and Figure 7.4. One can see from this analysis that the observed particle concentrations

Table 7.2: Evolution of 4:18 ECZ due to coagulation

Hours	Mode I		Observation at 4:18	
	UCN remaining	VCN remaining	UCN	VCN
- 9	1.2 x 10^6	360		
0	34,200	4,000	34,000 (mode I)	4,000 (mode I)
+ 6	16,000	4,700	16,000 (mode II)	11,600 (mode II)
+ 20	5,200	4,300		
+ 100	300	1,900		
+ 200	55	1,060		

(time = 0 hours) could have evolved from a "nucleation" event about 9 hours earlier than

our observations, i.e., about 5 PM local time on 6/12/92, just preceding sunset. At time =

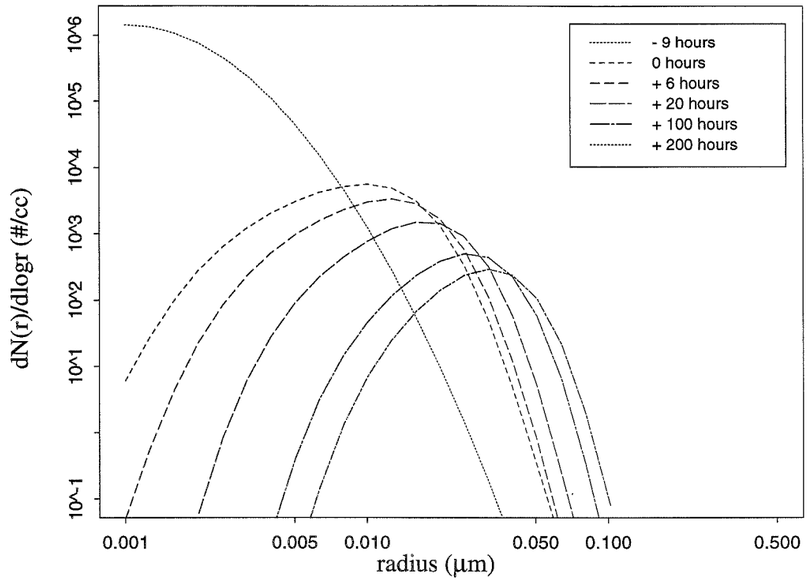

Figure 7.4 Evolution of size distribution via coagulation for 4:18 ECZ. Input parameters: σ=1.85, r_1=1 nm, ρ_{part}=1.3 g/cc.

- 9 hours, the peak of the particle distribution has a radius of 1 nm with the tail of the distribution in the CN size range (diameter > 15 nm). The magnitude of the concentration in the CN tail depends on the initial concentration and the standard deviation of the distribution. The concentration of CN is smallest for very high initial concentrations in a sharply peaked distribution.

The tail of 360 VCN/cc for the 1.85 standard deviation case is not representative of freshly nucleated particles. Nucleation cannot occur in the presence of high existing surface area, because gases will condense on previously existing particles rather than forming new particles. Therefore, a large nucleation event must happen quickly producing many particles of very small sizes. If this is the case, then the initial size distribution in the modelled evolution of the 4:18 ECZ is unrealistic as a nucleation event. I will complete plausibility calculations in Section 7.3.2.

There are two modes in the observed 4:18 ECZ. This coagulation analysis explains only one of them. Interestingly, mode II of the 4:18 ECZ cannot form due to coagulation from the same initial conditions which produce mode I (Table 7.2). This suggests that there must be processes other than coagulation which grow ultrafine particles into the CN size range without depleting the total particle concentration as dramatically as coagulation does. It is not clear from this analysis why two modes are observed side-by-side or exactly how these two modes evolve.

The products of this hypothetical "nucleation" event can evolve via coagulation into the observed concentrations at 4:18. The observed concentrations then continue to evolve due to coagulation, although the magnitude of the changes slows down significantly. After 200 hours, the VCN concentration is still higher than background levels. This means that, although coagulation can be largely responsible for the initial evolution of nucleation products, other processes must contribute to decreasing elevated particle concentrations to background levels.

7.3.2 Validity of coagulation results

I would like to explain why a distribution tail might exist near newly nucleated particles. This can be done analytically by considering the equations which govern nucleation and gaseous deposition and thus determining the relative dominance of these two processes compared to coagulation in the observed environment. The two questions I will address are:

1. Do particles grow from r_0 (1 nm) to r_{VCN} (10 nm) by diffusion or coagulation?
2. Is nucleation quenched when N_{VCN} (360/cc) particles have reached size r_{VCN}?

We can address question (1) by comparing the characteristic times for gaseous diffusion and coagulation to grow particles from r_0 to r_{VCN}. We can address question (2) by comparing characteristic times for depletion of gases by deposition onto r_{VCN}-sized particles and for depletion of gases due to nucleation of r_0-sized particles under the same set of conditions. These calculations can only yield order of magnitude estimates because of the number of assumptions used. But, if the compared times are different by at least one order of magnitude, we can determine the dominant process with some confidence.

I find coagulation times using Jensen's model. I want to find the time associated with forming 360/cc 10 nm radius particles from 1 nm particles. For these model runs, I use a standard deviation of 1.6 in order that no VCN tail exists at the beginning of the run; a particle mass density of 1.4 g/cc as obtained from Coffman's (1995) nucleation model for newly nucleated particles; a temperature of 8° C; and a pressure of 737 mb. The results yield a range of times from 2.5 hours to 70 hours depending on the initial concentration of UCN (Table 7.3).

Table 7.3: Evolution of N_{UCN} to 360/cc VCN due to coagulation

Initial UCN (#/cc)	Time to create 360/cc VCN (hours)
290,000	70
470,000	30
590,000	20
880,000	10
1.2×10^6	6
1.5×10^6	4
1.8×10^6	2.5

Diffusive growth is due to the gradient in gas concentration between the particle surface and the surrounding environment. Assuming our particles are initially composed of H_2SO_4 and H_2O, we have

$$\frac{dS_g}{dt} = -4\pi r_0 n_0 D_g S_g \equiv -\frac{S_g}{\tau_g}, \tag{7-1}$$

for g denoting H_2SO_4 or H_2O_{vap}. As the particle size changes due to diffusion, τ_g will change. I use this information to solve the equation for particle growth due to diffusion of H_2SO_4 and H_2O_{vap} (Equation 7-2) iteratively.

$$\frac{1}{2}\frac{dr^2}{dt} = \frac{\rho_{sat}^{H_2O}}{\rho_L} D_{H_2O} S_{H_2O} + \frac{\rho_{sat}^{H_2SO_4}}{\rho_L} D_{H_2SO_4} S_{H_2SO_4} \tag{7-2}$$

The end result of this analysis is a value for particle radius after diffusion of H_2SO_4 and H_2O_{vap} to the initial particles over time.

In order to complete this analysis I use the following values for the necessary variables:

$D_{H2O}=2.5 \times 10^{-5}\ m^2/s$

$$D_{H_2SO_4} = D_{H_2O}\sqrt{\frac{M_{H_2O}}{M_{H_2SO_4}}} = 1.1\times 10^{-5} m^2/s$$

$$\rho_{sat}^{H_2O} = \frac{\rho_{env}^{H_2O}}{S_{H_2O}(0)+1} = 3.8\times 10^{-4} kg/m^3 \text{ for } q_v = 1.2 \text{ g/kg}$$

$$\rho_{sat}^{H_2SO_4} = \frac{\rho_{env}^{H_2SO_4}}{S_{H_2SO_4}(0)+1} = 1.7 \times 10^{-13} kg/m^3 \text{ for 1 pptv } H_2SO_4$$

$S_{H2O}(0) = 0$ (D. Coffman, personal communication)

$S_{H2SO4}(0) = 23.5$ (D. Coffman, personal communication for binary nucleation when 1 pptv of H_2SO_4 is present.)

$\rho_L = 1400\ kg/m^3$ (D. Coffman, personal communication)

$r_o = 1$ nm

$n_o = 1 \times 10^6$/cc

This calculation is completed iteratively for a 10 second time interval and various concentrations of H_2SO_4 in the surrounding environment (Figure 7.5).

The results indicate that diffusive particle growth is very significant, even for low concentrations of H_2SO_4. In fact, for H_2SO_4 concentrations of 0.6 pptv, all of the 1×10^6/cc 1 nm particles grow to VCN size in under one hour. This implies that nucleation products grow rapidly into the CN size range due to diffusion.

These results suggest that gaseous deposition could easily cause particles to grow from the UCN size range to the VCN size range in short periods of time, thus producing the VCN tail discussed in relation to the formation of the 4:18 ECZ due to coagulation.

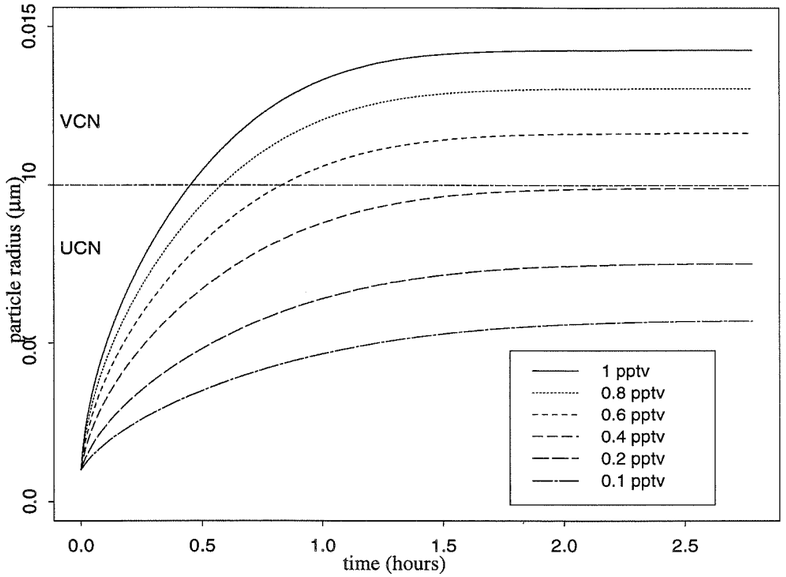

Figure 7.5 Particle growth due to diffusion of sulfuric acid. This calculation is done for an initial particle size of 1 nm and particle concentration of 1×10^6/cc.

The difficulty with this result is that all particles are grown out of the ultrafine size range, whereas significant UCN concentrations are observed in the ECZs. This inconsistency may be due to the fact that, (1) this calculation assumes that the gases diffuse to all particles equally or (2) that this calculation assumes all particles are initially nucleated at one time, as opposed including a nucleation rate which is a function of time.

This then leads us to the second question: is nucleation quenched by the time 360/cc VCN sized particles are formed?

In order to assess whether nucleation is still occurring once 360 VCN/cc are present, we compare the characteristic time for depletion of H_2SO_4 due to deposition onto N_{VCN} to the characteristic time for depletion of H_2SO_4 due to nucleation of 1 nm particles. The equations which describe these two processes are:

$$\tau_{diff}^{-1} = 4\pi D_g N_{VCN} r_{VCN} \ ; \ \tau_{nucl}^{-1} = J_{nucl} 4\pi r_0^3 \frac{\rho_{cond}^g}{3\rho_g}. \qquad (7\text{-}3)$$

From these calculations, I find a value for τ_{diff} of 0.6 hours. For the same conditions discussed for the diffusion/coagulation comparison, the nucleation rate, J_{nucl}, would have to be 360/cc-s, in order for $\tau_{diff}=\tau_{nucl}$. This rate is orders of magnitude higher than any of the rates which D. Coffman calculated for the conditions at ECZ 4:18. We can therefore conclude that nucleation is quenched by the time 360 VCN/cc are present.

These results imply that evolution of particles from size r_0 to r_{VCN} is dominated by diffusion and that nucleation is quenched by the time 360 VCN/cc are present. This leads me to conclude that the VCN tail described in the coagulation analysis is not part of a single nucleation event. Rather, the VCN tail of 360 VCN/cc has another source, possibly the juxtaposition of background particle concentrations and nucleation products after nucleation has ceased. This latter theory is difficult to quantify because the resolution of back trajectory routines is more coarse than the nucleation events themselves.

7.3.3 Transport of particles which compose ECZs

In this section I will summarize ECZ transport as discussed in Section 5.6.1 and Section 6.6.1. I will discuss vertical and horizontal transport in terms of characteristic times: for horizontal transport, I will consider transport across ECZ boundaries; for vertical transport, I will consider transport from the ECZ to above the inversion. Times with a positive sign following them indicate that transport serves as a source over the region of interest; a negative sign indicates a sink. Table 7.4 and the following statements summarize transport related to ECZs.

1. The particles in ECZs undergo rapid mean transport in both the horizontal and vertical direction.

2. The characteristic times are comparable on June 10 and during L1, although the June 10 times are consistently a bit shorter.

3. Mean vertical transport is consistently directed downwards serving as a source of particles for the lower FT. UCN are transported more rapidly than VCN. Unexpectedly, RCN mean vertical transport is rapid as well, especially during L1. This is due to very low RCN vertical fluxes near the inversion on June 13 which create a large flux gradient despite the fact that there is no peak in RCN concentrations during the 4:18 ECZ.

Table 7.4: ECZ time scales

date/time	τ_{mean} (hours) * = turbulent time dominates			$\tau_{turbulent}$ (hours) lo: f < 0.1/km; hi: f > 0.1/km		
	RCN	VCN	UCN	RCN	VCN	UCN
V: 6/10/92 5:30-9:43	3.1 (+)	1.4 (+)	NA	6.7 (+)	119 (+)	NA
H: 6/10/92 5:30-5:40	26 (-)	0.5 (-)	0.7 (-)	NA	NA	NA
V: 6/13/92 (1) 4:15-9:51	1.1 (+)	2.0 (+)	1.7 (+)	4.6 (-)	8.9 (-)	4.8 (-)
V: 6/13/92 (1) 4:15-10:03	1.3 (+)	2.1 (+)	1.8 (+)	5.1 (-)	9.3 (-)	5.0 (-)
H: 6/13/92 (1) 4:19-4:29	12 (-)	1.1 (-)	0.8 (-)	NA	NA	NA

The VCN fluxes near the inversion are quite a bit larger than either the RCN or UCN fluxes near the inversion, thus decreasing the VCN gradient and lengthening the VCN transport time relative to that for UCN and RCN. The UCN and RCN fluxes near the inversion are small because the UCN and RCN particle concentrations are very low.

4. Rapid horizontal transport for ultrafine and volatile particles indicates that ECZ characteristics will rapidly move downwind of the observed ECZ.

5. Turbulent vertical particle fluxes are generally positive for ECZs. Therefore turbulent mixing serves as a particle sink for the lower FT (as indicated by minus signs in Table 7.4), although the strength of this sink is small compared to the effect of mean transport.

6. The transport times involving the 5:37 ECZ on June 10 illustrate that UCN and VCN are undergoing more rapid transport than the refractory particles. This is consistent with the fact that the particle concentration is most peaked in the ultrafine and volatile CN components, and not so much in the surface derived component.

These results are consistent with the notion that nucleation products (very small, volatile particles) are being transported downwards due to mean motions and that, at times, vertical mixing due to turbulent motions is significant. We also see that turbulent

motions are most often significant for length scales longer than 10 km. This is particularly interesting because, for the two ECZs with total concentrations greater than 10,000/cc, the observed horizontal transect is only approximately 15 km. This would imply that the entire region will move relative to other air masses rather than experiencing dispersion due to small scale eddies.

7.3.4 Dispersion of particles

Transport analysis indicates that small scale eddies do not have a significant impact on turbulent mixing. Dispersion analysis should support this hypothesis. Particle dispersion can be assessed according to the procedure outlined in Section 4.2. This analysis yields a "diffusion coefficient" of 77 m^2/s for horizontal eddies with a spatial scale of 1 km in the upper regions of the free troposphere. With a value of K, one can calculate a dispersion time scale according to the diffusion equation (Equation 7-4).

$$\frac{\partial n}{\partial t} = K\nabla^2 n \qquad (7\text{-}4)$$

The results of this analysis procedure indicate that dispersion only occurs over very short distances and does not occur very quickly. For example, it takes about 3 hours for the particle concentration to disperse 1 km in the horizontal direction. The time scale increases rapidly with increasing spreading distance, L, according to $\tau \sim L^2/K$. This analysis illustrates that dispersion is not causing a significant amount of spreading of particles on spatial scales of 1 km in keeping with the evidence from the transport analysis.

7.4 Conclusions about ECZs

The previous discussion serves to illustrate the following points:

1. Observed ECZs are likely the result of nucleation occurring ~9 hours prior to observation. This implies (in the two ECZs with highest concentrations) that nucleation occurred just before sunset in the north central Atlantic.

2. Coagulation is a major sink process for newly nucleated particles, thus allowing the nucleation products to evolve into larger particles which are observed as ECZs.

3. Mean vertical winds transport particles downward toward the inversion on the same time scale as the size distribution evolves via coagulation.

4. Vertical turbulent mixing is a small effect, mixing particles both upward and downward.

5. Upper free tropospheric air is transported rapidly downward, regardless of whether the calculated fluxes incorporate a large ECZ.

6. Mean horizontal transport is only rapid across ECZ boundaries where particle gradients are large.

7. Growth of newly nucleated particles due to gaseous deposition is as or more significant than growth due to coagulation.

Nucleation and coagulation do not fully explain observed ECZs and background particle concentrations for two reasons. For one, nucleation products do not have as broad a size distribution as is necessary to create observed ECZs via coagulation. This broad distribution may not be due to nucleation itself but rather due to transport of newly nucleated particles into an adjacent region with background concentrations of larger particles. The second reason why nucleation and coagulation do not explain observed concentrations is that coagulation alone does not reduce particle concentrations in ECZs to background concentrations. The dominance of transport terms leads me to suggest that dynamical processes contribute to particle evolution. Turbulent vertical transport is important, which may serve to mix the concentrations at the ECZs vertically. Horizontal mixing may be important as well, especially since background particle concentrations are horizontally uniform and ECZs are not, but the existing data set does not allow us to explore this idea.

In the next chapter I will incorporate the background particle information (Chapter 5 and Chapter 6) with the ECZ analysis to create budgets of volatile and refractory particles.

Chapter 8: Budget Analysis

Using the observations discussed in previous chapters and analysis of the various particle processes, we can estimate budgets for particles in the marine atmosphere. The particle budget assesses the contributions of all particle processes to the time rate of change of particle concentrations. This analysis requires a Lagrangian reference frame, so I will focus only on those results obtained during L1.

8.1 METHODOLOGY

For the budget analysis, I split L1 into four periods: I. June 12, 16:00-22:00; II. June 13, 4:00-6:30 (ECZ); III. June 13, 6:30-10:30; IV. June 13, 16:00-22:00. I also divide the atmosphere into vertical layers which are each relatively uniform: upper FT, 720-820 mb; lower FT, 820-890 mb; cloud top region, 890 mb to cloud top (CT); upper MBL, CT to 990 mb; and lower MBL, 990-1020 mb (see Figure 8.1). Within each region

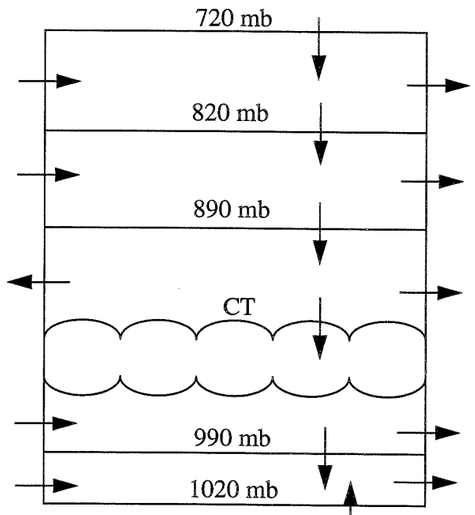

Figure 8.1 Schematic representation of layers used in budget study. Budget is computed using fluxes in and out of each box as indicated by arrows (direction of arrows is only illustrative in this figure).

I find the mean volatile and refractory particle concentrations. I then try to assess characteristic times for each observable process within each box. This requires a fair amount of approximation.

I do not have flux measurements at the boundaries of every box. Consequently, I have to interpolate from those fluxes which are available. For vertical fluxes there are enough measurements that the interpolation is probably quite reliable. Horizontal fluxes are only used from crosswind flight segments, of which there are relatively few. The paucity of data points for horizontal transport creates large uncertainties in the characteristic times associated with these fluxes. In most cases, turbulent vertical transport is not significant compared to mean transport. There are no processes other than transport which are calculated with enough frequency to include in the overall budget. When transport times are insignificant or deemed unreliable, they are not included in the budget tables (Table 8.1 and Table 8.2).

Using calculated time scales for various particle processes (Chapters 5-7), we can calculate an overall characteristic time scale for observable processes at one time.

$$\frac{1}{\tau_{tot,obs}} = \frac{1}{\tau_1} + \frac{1}{\tau_2} + \ldots \qquad (8\text{-}1)$$

The observable processes are likely not all of the important processes. We therefore calculate the characteristic time necessary to create the observed particle concentration at time, t_2, from that at time, t_1, according to the following equation.

$$\bar{n}(t_2)_{obs} = \bar{n}(t_1)_{obs} \exp\left(\frac{t_2 - t_1}{\tau_{tot}}\right) \qquad (8\text{-}2)$$

The difference between $1/\tau_{tot}$ and $1/\tau_{tot,obs}$ is the inverse of the characteristic time for particle processes for which we have been unable to account. I will represent this missing source or sink term by its characteristic time, τ^*. The magnitude of τ^* and its sign, i.e., the identification of the process as a source or a sink, tell us about the importance of unmeasured processes (i.e., non-transport processes) and perhaps give us clues as to the nature of these processes.

In the budget tables, positive signs represent source terms in the box of interest, and negative signs represent sink terms in the box of interest. The computed concentrations at time, t_2, are calculated from Equation 8-2 using the observed particle concentration and characteristic time ($\tau_{tot,obs}$) at time t_1. These computed concentrations are indicated in the box at time t_2 and are placed below the observed concentration at time t_2. Missing terms indicated at time t_1 are those terms necessary to produce the observed concentration at time t_2 rather than the concentration computed from the observed transport and mixing processes.

8.2 VOLATILE PARTICLE BUDGET

The volatile particle budget is summarized in Table 8.1. The Δt values listed in Table 8.1 are the time difference between each of the four periods. From this table, we can see that there are missing sources below cloud and missing sinks above cloud of significant magnitude. These are discussed in the following paragraphs.

Above cloud (upper FT and lower FT) we are missing important sink terms except for one instance related to the 4:18 ECZ where we have missing source terms. Most importantly, we are missing large sink terms between periods III and IV. This is a time period when we move from high mean concentrations which are possibly related to nucleation to lower background concentrations. Evidently, mean transport processes cannot entirely account for this transition. Coagulation is certainly one sink, but for the mean concentrations treated in this budget, coagulation is quite slow. Only for the ECZs themselves is coagulation fast enough to alter the results presented here and that will not effect the III to IV transition. The other sinks which may be dominant are turbulent mixing processes which I have no measurement of in the horizontal plane and seem to be insignificant in the vertical plane. A well-constructed flight plan may be able to address turbulence more accurately (see Chapter 9).

The missing sink term in the cloud top region is possibly divergence at cloud top for Period I (Figure 8.2). This may occur in a Lagrangian mission because an aircraft is not entirely capable of staying with the same air mass. The reason there is a missing sink term is that downward fluxes due to mean winds are greater than entrainment fluxes at

Table 8.1: Volatile Particle Budget

	I 6/12 16:00-22:00	II 6/13 (1) 4:00-6:30	III 6/13 (1) 6:30-10:30	IV 6/13 (2) 16:00-22:30
Pressure (mb)	Δt=12 hours Δt=3 hours Δt=10 hours τ^*=unknown source or sink time scale necessary to balance budget			
720-820 upper FT	observed: 1700/cc $\tau_{\overline{w}\,\overline{n}}$ ~ 12 hr (+) $\tau_{\overline{u}\,\overline{n}}$ ~ 2.9 hr (+)	obs: 2300/cc comp: 22000/cc $\tau_{\overline{w}\,\overline{n}}$ ~ 1.8 hr (+) $\tau_{\overline{u}\,\overline{n}}$ ~ 1.1 hr (-) $\tau_{\overline{v}\,\overline{n}}$ ~ 14.8 hr (-) $\tau_{\overline{w'n'}}$ ~ 5.6 hr(-)	obs: 1800/cc computed: 400/cc $\tau_{\overline{w}\,\overline{n}}$ ~ 125 hr(+) $\tau_{\overline{u}\,\overline{n}}$ ~ 20 hr (-) [$\tau_{\overline{v}\,\overline{n}}$~ 0.9 hr (+)]	obs: 360/cc comp: ∞
need sink & source	τ^*~ 1.2 hr (–)	τ^*~ 2.0 hr (+)	τ^*~ 1.1 hr (–) τ^*~ 8.4(-) [w/o $\overline{vn}$]	
820-890 lower FT	obs: 400/cc $\tau_{\overline{w}\,\overline{n}}$~ 2.8 hr (+) $\tau_{\overline{u}\,\overline{n}}$~ 3 hr (+)	obs: 1000/cc comp: ∞ $\tau_{\overline{w}\,\overline{n}}$ ~ 1.9 hr (+) $\tau_{\overline{u}\,\overline{n}}$ ~ 2 hr (-) $\tau_{\overline{v}\,\overline{n}}$ ~ 4.2 hr (-)	obs: 450/cc comp: 530/cc $\tau_{\overline{w}\,\overline{n}}$~ 29 hr (+) $\tau_{\overline{u}\,\overline{n}}$~ 20 hr (+) [$\tau_{\overline{v}\,\overline{n}}$~ 0.3 hr (+)]	obs: 360/cc comp: ∞
need sink & source	τ^*~ 1.6 (–)	τ^*~ 18.7 hr (-)	τ^*~ 0.29 hr (-) τ^*~ 9.3(-) [w/o $\overline{vn}$]	
890-CT CT region	obs: 420/cc $\tau_{\overline{w}\,\overline{n}}$ ~ 17 hr (+) $\tau_{\overline{u}\,\overline{n}}$~ 3.7 hr (+)	obs: 300/cc comp: ∞ $\tau_{\overline{w}\,\overline{n}}$ ~ 11 hr (+) $\tau_{\overline{v}\,\overline{n}}$~ 2.2 hr (-)	obs: 260/cc comp: 5500/cc $\tau_{\overline{w}\,\overline{n}}$ ~ 6 hr (-) $\tau_{\overline{u}\,\overline{n}}$ ~ 11 hr (+) [$\tau_{\overline{v}\,\overline{n}}$ ~ 0.13 hr(+)]	obs: 400/cc comp: ∞
need sink & source	τ^*~ 2.8 hr (–) cloud: 970-990 mb	τ^*~ 3.2 hr (+) cloud: 950-980 mb	τ^*~8.4(+) [w/o $\overline{v}\,\overline{n}$] cloud: 940-975 mb	cloud: 900-920 mb
CT-990 upper MBL	obs: 120/cc $\tau_{\overline{w}\,\overline{n}}$ ~ 0.8 hr (-)	obs: 50/cc comp: 0/cc $\tau_{\overline{w}\,\overline{n}}$ ~ 1.1 hr (-) $\tau_{\overline{v}\,\overline{n}}$ ~ 4.6 hr (-)	obs: 90/cc comp: 2/cc $\tau_{\overline{w}\,\overline{n}}$ ~ 9.5 hr (-) $\tau_{\overline{v}\,\overline{n}}$ ~ 1.1 hr (-)	obs: 115/cc comp: 0/cc
need source	τ^*~ 0.85 hr (+)	τ^*~ 0.76 hr (+)	τ^*~ 0.98 hr (+)	
990-1020 lower MBL	obs: 160/cc $\tau_{\overline{w}\,\overline{n}}$ ~ 2.2 hr (+) $\tau_{\overline{u}\,\overline{n}}$ ~ 3 hr (+)	obs: 70/cc comp: ∞ $\tau_{\overline{w}\,\overline{n}}$ ~ 5.8 hr (+) $\tau_{\overline{u}\,\overline{n}}$~ 2.8 hr (-)	obs: 100/cc comp: 93/cc $\tau_{\overline{w}\,\overline{n}}$ ~ 2.4 hr (-)	obs: 115/cc comp: 2/cc
need source	τ^*~ 1.2 hr (–)	τ^*~ 41 hr (+)	τ^*~ 2.3 hr (+)	

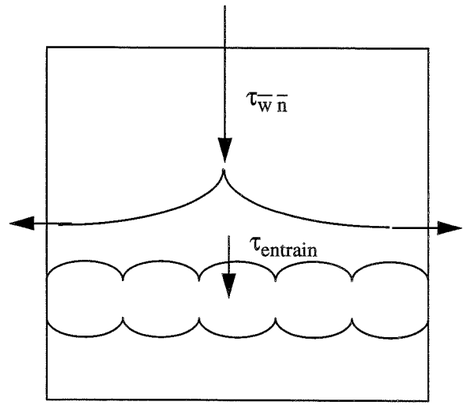

Figure 8.2 Schematic of cloud top divergence in an Eulerian reference frame. The relative length of vertical transport and entrainment arrows indicate that a sink is necessary in this region.

cloud top. Horizontal outflow at cloud top would provide a sink in the observation region. The possibility of horizontal divergence should be addressed in future studies.

During Periods II and III, there are missing source terms at cloud top. This may be due to cloud top nucleation (Hegg *et. al.*, 1990) or horizontal influx of particles from adjacent regions. It is also possible that this result is due to erroneous high particle concentrations just above cloud top.

There is one period in the upper FT for which we are missing a source term. This is the period which subsumes the 4:18 ECZ. This is due to very fast mean horizontal transport out of this region as taken on the flight leg from which we observe the 4:18 ECZ. Because this value is taken from a locally anomalous region, it is likely not accurate for the entire box. If we neglect this term, we find that we are missing a sink term rather than a source term of magnitude 2.6 hours which is consistent with the missing sink terms for the other periods and regions in the FT.

Below cloud we are consistently missing source terms of significant magnitude. One possible difficulty in this region is the erroneous nature of particle concentrations near and in cloud. Although I have tried to remove this effect (Section 4.1) it is possible

that the particle concentrations which remain are not representative of the actual environment and produce erroneous signals in the budget. Another related effect is the fact that we cannot accurately assess cloud processes. Although the dominant effect of a cloud is as a particle sink, it is possible that we are missing some cloud-related sources as well. Finally, though, the lack of measurements of terms related to mixing in the MBL is a stumbling block. As long as there is a persistent cloud topped boundary layer, there is mixing within the MBL, but we have few measurements of the strength of this effect and what measurements we have are too slow to be effective. This suggests that we need to obtain more measurements of turbulent mixing in order to increase the reliability of the results and further constrain the budget calculations.

The possible volatile particle sources within the MBL are low-level constant nucleation (Coffman and Hegg, 1995) or influx of organic particles from the sea surface (Novakov and Penner, 1993).

In the volatile particle budget I have included terms due to mean vertical transport which may be erroneous. If I re-do the budget study neglecting mean vertical transport times due to their uncertainty, τ^* is changed in magnitude but not in its effect (i.e., serving as a source or a sink) in all cases except three. This indicates that the discussion of source and sink terms in the previous paragraphs still holds true but that some of the missing sources and sinks may be explained by mean vertical transport. This procedure can put constraints on the accuracy of mean vertical fluxes.

8.3 Refractory particle budget

The refractory particle budget is summarized in Table 8.2. Particles which are derived from surface sources (dust, ash, sea salt) are refractory in nature, i.e., they do not burn off when heated to 300°C. Therefore, I will describe the refractory particle budget as a budget of surface-derived particles. For refractory particles we are primarily (although not exclusively) missing sinks above cloud and sources below as is the case for the volatile particle budget.

In the FT, the refractory budget uncovers missing sinks during periods I, and sources in period II and III. For period I, mean vertical and crosswind transport in the

Table 8.2: Refractory Particle Budget

	I 6/12 16:00-22:00	II 6/13 (1) 4:00-6:30	III 6/13 (1) 6:30-10:30	IV 6/13 (2) 16:00-22:30
Pressure (mb)	Δt=12 hours Δt=3 hours Δt=10 hours τ^*=unknown source or sink time scale necessary to balance budget			
720-820 upper FT *need sink & source*	observed: 80/cc $\tau_{\overline{w}\,\overline{n}}$ ~ 18.5 hr (+) $\tau_{\overline{u}\,\overline{n}}$ ~ 21 hr (-) τ^*~ 56.9 hr (–)	obs: 70/cc computed: 86/cc $\tau_{\overline{w}\,\overline{n}}$ ~ 0.35 hr (+) $\tau_{\overline{u}\,\overline{n}}$ ~ 23 hr (+) $\tau_{\overline{v}\,\overline{n}}$ ~ 125 hr (-) τ^*~ 0.3 hr (-)	obs: 45/cc comp: ∞ $\tau_{\overline{w}\,\overline{n}}$ ~ 31 hr(+) [$\tau_{\overline{v}\,\overline{n}}$ ~ 2.2 hr (-)] τ^*~ 4.5 (+) τ^*~ 17(+) [no $\overline{v}\,\overline{n}$]	obs: 110/cc comp: 12/cc
820-890 lower FT *need source*	obs: 30/cc $\tau_{\overline{w}\,\overline{n}}$ ~ 8.3 hr (+) τ^*~ 11.5 (–)	obs: 45/cc comp: 130/cc $\tau_{\overline{w}\,\overline{n}}$ ~ 7.3 hr (+) $\tau_{\overline{v}\,\overline{n}}$~ 6.2 hr (-) τ^*~ 16.8 hr (+)	obs: 50/cc comp: 42/cc $\tau_{\overline{w}\,\overline{n}}$ ~ 3.7 hr (+) $\tau_{\overline{u}\,\overline{n}}$ ~ 5.6 hr (+) [$\tau_{\overline{v}\,\overline{n}}$ ~ 1.2 hr (-)] τ^*~ 1.5 hr (+) τ^*~ 2.5(–) [no $\overline{v}\,\overline{n}$]	obs: 80/cc comp: 0/cc
890-CT CT region *need sink & source*	obs: 300/cc $\tau_{\overline{w}\,\overline{n}}$ ~ 5.3 hr (-) $\tau_{\overline{u}\,\overline{n}}$ ~ 4 hr (+) τ^*~ 12.5 hr (–) cloud: 970-990 mb	obs: 240/cc comp: 10000/cc $\tau_{\overline{w}\,\overline{n}}$ ~ 4.4 hr (-) $\tau_{\overline{v}\,\overline{n}}$ ~ 20 hr (-) τ^*~ 6.2 hr (+) cloud: 950-980 mb	obs: 170/cc comp: 325/cc $\tau_{\overline{w}\,\overline{n}}$ ~ 2.6 hr (-) $\tau_{\overline{u}\,\overline{n}}$ ~ 31 hr (+) $\tau_{\overline{v}\,\overline{n}}$ ~ 2.8 hr (-) τ^*~ 1.3 hr (+) cloud: 940-975 mb	obs: 260/cc comp: 40/cc cloud: 900-920 mb
CT-990 upper MBL *need source*	obs: 150/cc $\tau_{\overline{w}\,\overline{n}}$ ~ 0.64 hr (-) τ^*~ 0.7 hr (+)	obs: 35/cc comp: 0/cc $\tau_{\overline{w}\,\overline{n}}$ ~ 1.1 hr (-) $\tau_{\overline{v}\,\overline{n}}$ ~ 20 hr (-) τ^*~ 0.9 hr (+)	obs: 55/cc comp: 2/cc $\tau_{\overline{w}\,\overline{n}}$ ~ 0.8 hr (-) $\tau_{\overline{v}\,\overline{n}}$ ~ 2.8 hr (-) τ^*~ 0.6 (+)	obs: 135/cc comp: 0/cc
990-1020 lower MBL *need source*	obs: 145/cc $\tau_{\overline{w}\,\overline{n}}$ ~ ∞ $\tau_{\overline{w'n'}}$ ~ 7.1 hr (-) τ^*~ 16.6 hr (+)	obs: 55/cc comp: 30/cc $\tau_{\overline{w}\,\overline{n}}$ ~ 0.3 hr (-) $\tau_{\overline{u}\,\overline{n}}$ ~ 7.3 hr (+) $\tau_{\overline{v}\,\overline{n}}$ ~ 7.6 hr (-) τ^*~ 0.27 (+)	obs: 150/cc comp: 0/cc $\tau_{\overline{w}\,\overline{n}}$ ~ 1.6 hr (+) $\tau_{\overline{u}\,\overline{n}}$ ~ 78 hr (+) $\tau_{\overline{v}\,\overline{n}}$ ~ 0.8 hr (-) $\tau_{\overline{w'n'}}$ ~ 7.8 hr(+) τ^*~ 2.1 hr (+)	obs: 135/cc comp: 2/cc

upper FT account for the observed concentration in period II within 25%. This is true in the lower FT between periods II and III as well. We are missing a large sink in the period which is upper bounded by the 4:18 ECZ. Even though RCN concentrations are not particularly elevated in this region, there is still very strong downward transport into this region from the 4:18 ECZ which must be countered by a sink term.

We are missing large sources between periods III and IV in the FT. During this transition, in contrast to the volatile budget case, we are moving from a region of low concentration to high concentration. Mean transport does not appear to account for this change. Perhaps there is some source moving relative to the Lagrangian reference frame in this period, such as a bit of dust. We have no way of determining exactly what this source is given the limitations of the ASTEX data set.

In the cloud top region we are missing sink terms for period I. This sink term is probably divergence for the same reasons discussed in Section 8.2. For periods II and III in the cloud top region, we find that we are missing a source term of moderate strength. This may be due to horizontal transport of particles into this region from adjacent regions. This result may be consistent with cloud top divergence early in the Lagrangian which serves as a source of particles later in the Lagrangian (assuming the Lagrangian mission is not perfectly sampling only one air mass).

Below cloud we are missing source terms of significant magnitude except in one instance (period I to period II) when the budget is approximately balanced (within 25%) due to vertical mixing. The most probable source, and one to which we have not been able to attribute a strength, is sea salt. From the correlation analysis presented in Figure 6.8, we might expect a portion of the observed RCN concentration near the surface to be sea salt. Because the sea salt source is sporadic, we cannot assign a magnitude to the sea salt flux. But, we do see the largest discrepancy between observed concentrations and computed concentrations in periods III and IV. We might therefore conclude that during these periods the sporadic sea salt source is most active. Why, though, isn't this accounted for in the transport terms? Possibly because the source is at the surface and the lowest flight legs are at 50 m. It is unclear what happens to the particles between the surface and 50 m

but perhaps the source products are sufficiently diffuse at 50 m that we cannot see their signature in flux calculations.

As in the volatile budget, I include mean vertical transport in the previous analysis. If I neglect these terms due to uncertainties I find, as in the volatile budget, that the missing terms are not altered in terms of their role as sources and sinks except in three cases. Therefore, the discussion above could be modified by the possibility that the missing sources and sinks are due to mean vertical transport.

The results discussed in the preceding sections are summarized in Figure 8.3. The source and sink strengths are calculated from $\bar{n}/\tau^*$ which values are indicated in Table 8.1 and Table 8.2. The uncertainty in the source and sink strengths is approximately 70% of the value indicated in Figure 8.3. This uncertainty is large but will not alter the designation of each term as a source or a sink, only the magnitude.

8.4 Budget Conclusions

The budget calculations contained in the preceding pages illuminate a number of important points which must be addressed if we are to complete an accurate particle budget using future data sets. First, we must devise an accurate way to assess turbulent mixing and divergence. This can be accomplished with a carefully devised flight plan. We need to assess errors in mean vertical transport. We also need to assess the magnitude of the sea salt source. This can be done approximately with shipboard instrumentation. And, from the ECZ analysis it is evident that diffusive growth of particles may be very significant. Analysis of diffusion requires spatially-resolved gas concentrations. Detailed proposals for future work will be included in Chapter 9.

The consistent presence of a volatile particle source in the MBL due to processes other than measurable transport indicates that transport from the FT is not the only source of volatile particles in the MBL. There must be in situ volatile particle sources as well such as low-level nucleation and organic emissions. In-cloud particle measurements as well as information about horizontal mixing in the MBL will further define the strength of the in situ volatile particle source as compared to the free tropospheric source.

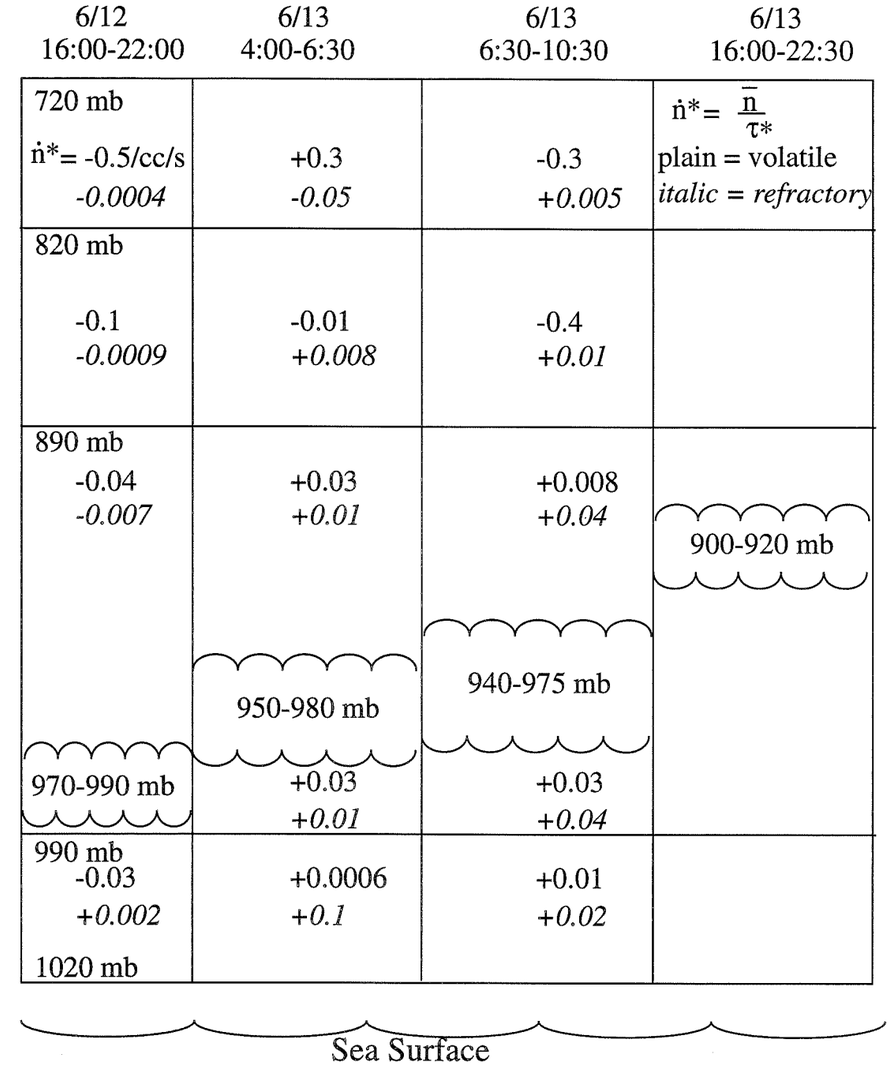

Figure 8.3 Summary of budget results. Source and sink strengths for volatile and refractory particles are represented in plain text and italicized text, respectively.

Chapter 9: Conclusions and Future Work

The goal of this study was to quantify which particle processes are the most important determinants of particle concentration, size, and composition in the remote marine atmosphere. Within the constraints of existing data sets, this goal was achieved. In the following paragraphs I will discuss the conclusions I was able to draw and the inferences I made in order to explain observed particle evolution. This discussion of conclusions and inferences will be followed by ideas for future data acquisition and analysis which can further constrain the relative importance of various particle processes.

The discussion of elevated concentration zones (ECZs) leads me to conclude that large, sporadic nucleation events occur in the upper free troposphere. These events occur in late afternoon perhaps due to H_2SO_4 accumulation throughout the daylight hours. The newly nucleated particles then evolve due to coagulation and gaseous deposition.

Large-scale, downward transport is a consistent feature in the unpolluted ASTEX environment if we do not include an offset in the measured vertical winds. This transport brings nucleation products from the upper free troposphere to the inversion providing a significant source of particles to the lower free troposphere. This source must be balanced by unmeasured sinks in the free troposphere. The most likely candidates for free tropospheric particle sinks are coagulation and turbulent mixing. Cloud top entrainment serves as a small sink for free tropospheric particles.

Within the marine boundary layer, transport calculations consistently do not account for sources of volatile and refractory particles. The candidates for marine boundary layer particle sources are surface production of sea salt and organics and low-level, persistent nucleation as discussed by Coffman and Hegg, 1995.

Each of the processes mentioned above could be analyzed more thoroughly given some alterations in data acquisition.

Transport can be assessed more thoroughly given flight plans designed specifically for observing transport processes such as turbulent mixing and divergence. This is most easily accomplished through use of two aircraft flying with the same instrumentation. Two aircraft could simultaneously measure fluxes on box boundaries (as is necessary for

the budget calculations), and could quickly complete closed horizontal paths over which one could calculate divergence. Two aircraft would also acquire large amounts of data in a limited time, which is necessary to increase accuracy. Further assessment of vertical velocity uncertainties is crucial to future transport analyses.

I would also suggest that aircraft sample the free troposphere frequently at various times of day with the hope of observing more cases of nucleation products, i.e., ECZs. Once an ECZ is found, the flight plan should be altered in order to intersect the ECZ periodically. This would enable one to observe the evolution of recently nucleated particles, and perhaps validate my conclusions regarding coagulation and gaseous deposition as dominant methods of particle evolution.

Instrumentation capable of measuring H_2SO_4 and NH_3 concentrations would allow more accurate analysis of nucleation rates and gaseous deposition rates. And, a method for detemining sea salt fluxes more accurately, i.e. measurements taken closer to the surface, is desireable. I do not think aircraft can accomplish this.

There is clearly a lot more work which can be done to further our understanding of submicron particle processes in the remote marine environment. The budget study approach used here has proven very fruitful and with improved data sets will provide further illumination of important particle processes.

Bibliography

Blomquist, B. W., A. R. Bandy, and D. C. Thornton, 1995: Sulfur gas measurements in the eastern North Atlantic Ocean during ASTEX/MAGE. *J. Geophys. Res.*, submitted.

Bluth, R. T., and B. A. Albrecht, 1993a: ASTEX/MAGE experiment summary. Part I: Mission summaries. *Pennsylvania State University, Meteorology Department.*

Bluth, R. T., and B. A. Albrecht, 1993b: ASTEX/MAGE experiment summary. Part II: Platform operations. *Pennsylvania State University, Meteorology Department.*

Bretherton, C. S., and R. Pincus, 1995: Cloudiness and marine boundary layer dynamics in the ASTEX Lagrangian experiments. Part I: Synoptic setting and vertical structure. *J. Atmos. Sci.*, accepted.

Bretherton, C. S., P. Austin, and S. T. Siems, 1995: Cloudiness and marine boundary layer dynamics in the ASTEX Lagrangian experiments. Part II: Cloudiness, drizzle, surface fluxes and entrainment. *J. Atmos. Sci.*, accepted.

Clarke, A. D., T. Uehara, and J. N. Porter, 1995: Atmospheric nuclei and related aerosol fields over the Atlantic: Clean subsiding air and continental polllution during ASTEX. *J. Geophys. Res.*, submitted. **check with Clarke**

Clarke, A. D., 1993: Atmospheric nuclei in the Pacific midtroposphere: Their nature, concentration, and evolution. *J. Geophys. Res.*, **98**, 20633-20647.

Clarke, A. D., 1991: A thermo-optic technique for *in-situ* analysis of size-resolved aerosol physicochemistry. *Atmos. Environ.*, **25A**, 635-644.

Coffman, D. and D. A. Hegg, 1995: A preliminary study of the effect of ammonia on particle nucleation in the marine boundary layer. *J. Geophys. Res.*, **100**, 7147-7160.

Covert, D. S., V. N. Kapustin, T. S. Bates, and P. K. Quinn, 1995: Physical properties of marine boundary layer aerosol particles of the mid-Pacific in relation to sources and meteorological transport. *J. Geophys. Res.*, submitted.

Fitzgerald, J. W., 1991: Marine aerosols: A review. *Atmos. Env.*, **25A**, 533-545.

Fuchs, N. A., 1964: *The Mechanics of Aerosols*. Dover Publications, New York, 408 pp.

Hegg, D. A., P. Yuen, and T. V. Larson, 1992a: Modeling the effects of heterogeneous cloud chemistry on the marine particle size distribution. *J. Geophys. Res.*, **97**, 12927-12933.

Hegg, D. A., D. S. Covert, and V. N. Kapustin, 1992b: Modeling a case of particle nucleation in the marine boundary layer. *J. Geophys. Res.*, **97**, 9851-9857.

Hegg, D. A., L. F. Radke, and P. V. Hobbs, 1990: Particle production associated with marine clouds. *J. Geophys. Res.*, **95**, 13917-13926.

Heintzenberg, J., 1989: Fine particles in the global troposphere: A review. *Tellus*, **41B**, 149-160.

Hobbs, P. V., 1993: *Aerosol, Cloud, Climate Interactions*. Academic Press, San Diego, 235 pp.

Hoppel, W. A., J. W. Fitzgerald, G. M. Frick, R. E. Larson, and E. J. Mack, 1990: Aerosol size distributions and optical properties found in the marine boundary layer over the Atlantic Ocean. *J. Geophys. Res.*, **95**, 3659-3686.

Huebert, B. J., L. Zhuang, S. Howell, K. Noone, and B. Noone, 1995: Sulfate, nitrate, methanesulfonate, chloride, ammonium, and sodium measurements from ship, island, and aircraft during ASTEX/MAGE. *J. Geophys. Res.*, submittted.

Lin, X., W. L. Chameides, C. S. Kiang, A. W. Stelson, and H. Berresheim, 1992: A model study of the formation of cloud condensation nuclei in remote marine areas. *J. Geophys. Res.*, **97**, 18161-18171.

Martin, G. M., D. W. Johnson, D. P. Rogers, P. R. Jonas, P. Minnis, and D. A. Hegg, 1995: Observations of the interaction between cumulus clouds and warm stratocumulus clouds in the marine boundary layer during ASTEX. *J. Geophys. Res.*, accepted.

Miller, E. R. and R. B. Friesen, 1988: Standard output data products from the NCAR research aviation facility. *NCAR Research Aviation Facility, Bulletin No. 9*, 1988.

Monahan, E. C., D. E. Spiel, and K. L. Davidson, 1986: A model of marine aerosol generation via whitecaps and wave disruption, pp. 167-174, in: *Oceanic Whitecaps,* E. C. Monahan and G. Mac Niocaill, eds., D. Reidel Publishing Company, Dordrecht, Holland.

Novakov, T. and J. E. Penner, 1993: Large contribution of organic aerosols to cloud-condensation-nuclei concentrations. *Nature*, **365**, 823-826.

O'Dowd, C. D., and M. H. Smith, 1993: Physicochemical properties of aerosols over tthe Northeast Atlantic: Evidence for wind-speed-related submicron sea-salt aerosol production. *J. Geophys. Res.*, **98**, 1137-1149.

Pasquill, F., 1974: *Atmospheric Diffusion: The Dispersion of Windborne Material from Industrial and other Sources.* Ellis Horwood Limited, Chichester, 429 pp.

Porter, J. N., A. D. Clarke, G. Ferry, and R. F. Pueschel, 1992: Aircraft studies of size-dependent aerosol sampling through inlets. *J. Geophys. Res.*, **97**, 3815-3824.

Pruppacher, H. R. and J. D. Klett, 1978: *Microphysics of Clouds and Precipitation.* D. Reidel Publishing Co., Dordrecht, 714 pp.

Raes, F., 1995: Entrainment of free tropospheric aerosols as a regulating mechanism for cloud condensation nuclei in the remote marine boundary layer. *J. Geophys. Res.*, **100**, 2893-2903.

Raes, F. and R. Van Dingenen, 1992: Simulations of condensation and cloud condensation nuclei from biogenic SO_2 in the remote marine boundary layer. *J. Geophys. Res.*, **97**, 12901-12912.

Sitarski, M., and J. H. Seinfeld, 1977: Brownian coagulation in the transition regime. *J. Colloid Interface Sci.*, **61**, 261-271.

Smith, M. H., P. M. Park, and I. E. Consterdine, 1993: Marine aerosol concentrations and estimated fluxes over the sea. *Quart. J. Roy. Met. Soc.*, **119**, 809-824.

Twomey, S., 1977: *Atmospheric aerosols.* Elsevier, Amsterdam, 302 pp.